A coupled model for the dynamics of gas exchanges in the human lung with Haldane and Bohr's effects

Laurent Boudin, Céline Grandmont, Bérénice Grec, Sébastien Martin

A COUPLED MODEL FOR THE DYNAMICS OF GAS EXCHANGES IN THE HUMAN LUNG WITH HALDANE AND BOHR'S EFFECTS

LAURENT BOUDIN, CÉLINE GRANDMONT, BÉRÉNICE GREC, AND SÉBASTIEN MARTIN

Abstract. We propose an integrated dynamical model for oxygen and carbon dioxide transfer from the lung into the blood, coupled with a lumped mechanical model for the ventilation process, for healthy patients as well as in pathological cases. In particular, we focus on the Bohr and Haldane effects, which induce a nonlinear coupling between the oxygen and the carbon dioxide. We also take into account the dead space volume, which requires a special attention in the pathological cases.

Contents

1. Introduction

The main function of the respiratory system is to ensure the oxygen transfer from the outside air to the blood and the carbon dioxide transfer from the blood to the outside air. Those transfers are achieved thanks to passive diffusion through the alveolo-capillary membrane which separates two phases: the alveolar air on the one side, the blood on the other side. Then, the gas exchanges at this level require air renewal, which happens during the mechanical ventilation process.

This process involves the air transport through the resistive bronchial tree, which irrigates the elastic lung tissue called parenchyma. Driven by the diaphragm contraction, the parenchyma is deformed, inducing a pressure drop between the alveoli and the mouth, and consequently an airflow. There is a hierarchy of models which can describe this phenomenon.

Models involving ODEs, possibly nonlinear and complex, may be considered, as the ones in [27, 30, 13, 19], using for example nonlinear double-balloon models. The air transport can further be described with unsteady one-dimensional advection-diffusion PDEs, see [19, 22, 23] for instance, and even with either unsteady systems describing the three-dimensional air flow, e.g. [2, 24], or a resistive tree interacting with a three-dimensional elasticity model as in [26, 6, 25].

In this paper, we choose to consider a simple mechanical model for the respiratory system similar to the ones from [3, 5, 4, 34]: a single-compartment model, often represented under the form of a balloon corresponding to the lungs, connected to a pipe representing the airways. There are mainly two physiological parameters involved in that model. The lung elastance E measures the stiffness related to stretching forces, so that the lung spontaneously comes back to rest. The pulmonary resistance R measures the resistive forces in the whole bronchial tree (due to the friction between the gas molecules and the airway walls) and the resistive forces to deformation inside tissues (due to the friction between the lung tissues and the chest wall). Those critical parameters are affected in pathological situations which can induce substantial modifications of the elastance (fibrosis, emphysema...), or the resistance (asthma, COPD...), but also of other physiological parameters.

The lung mechanical function is to serve as a pump for the air renewing to bring oxygen inside the lung and expel the carbon dioxide produced within the body. Thus we need to describe the dynamics of each species concentrations at the alveolar level, mainly driven by diffusion.

The gas exchanges occur through the alveolo-capillary membrane and, thus, may be widely affected by the so-called lung dead space, *i.e.* the volume of air not involved in the gas exchanges, see, for instance, [10, 34]. This dead space is the sum of the anatomic dead space and an extra volume depending on the patient state and on the breathing scenario. In particular, the air entering the alveoli during inspiration is a mixture of dead-space air, assumed to be filled of gases whose mole fractions are the current ones in the lung, and fresh air. Higher values of the dead space may have a strong impact on the air renewing and thus the gas transfer. Hence, it is crucial to properly model the dead space, and more precisely, in our model, the extra volume, which we call here the pathological dead space: it is close to zero when the patient is healthy, but can become significantly non-zero for asthmatic or emphysematous patients, for example.

The gaseous exchange involves a passive diffusion process through the alveolar membrane together with the binding of oxygen and carbon dioxide to hemoglobin. The diffusion process of both gases through the alveolar membrane is characterized by two constant diffusion coefficients, denoted by D_{m,O_2} and D_{m,CO_2}, related by $D_{m,\mathrm{CO}_2} = 20 D_{m,\mathrm{O}_2}$ [10], and is driven by the blood-alveolar pressure drops of each species. The affinity of hemoglobin with respect to oxygen depends on the blood pressure of carbon dioxide, referred to as the Haldane and Bohr effects in the literature, see [11, 28, 9, 10, 18]. Those effects induce a natural nonlinear coupling in the dynamics of the diffusion process of each species. Roughly speaking, Haldane's effect is due to the fact that the blood oxygen increases the carbon dioxide removal, and Bohr's refers to the shift of oxygen-binding affinity with respect to both pH and carbon dioxide concentration.

Consequently, the nonlinear coupled dynamics of the blood partial pressures of oxygen and carbon dioxide, based upon a concentration balance, may lead to substantial modifications of the gas transfer in pathological situations (e.g. in emphysema diffusion permeability are lowered, leading to possible kinetic limitation in the instantaneous gas transfer).

Note that very complex ODE systems modelling the whole respiratory process have also been proposed in the literature, as in [8]. Such systems include cardiovascular phenomena and central neural control. In this work, we aim to focus only on the ventilation-diffusion coupling with a limited number of physiological parameters, which can moreover be calibrated and physically interpreted. The paper is hence organised as follows. In Section 2, we present our simple ventilation-diffusion model, which can capture the main observable quantities for a healthy patient at rest. In Section 3, we further discuss the gas exchanges and provide a relevant model for both Bohr and Haldane effects. We then start the numerical studies by first investigating some reference situations for a

healthy patient in Section 4, which allows to check the relevant behaviour of our model. Next, in Section 5, we lead a sensitivity analysis with respect to the parameters R, E and D_m to study their influence on the gas transfer efficiency, in order to find possible global structuring or crossed effects with respect to those parameters. Eventually, Section 6 is dedicated to exploring the behaviour of our model in various pathological situations.

2. A 0D model for the respiratory system

2.1. **Mechanical model.** Let us first write the simple linear lung mechanical model we use here. As we already emphasized, it involves two main ingredients: the resistance R of the branches connecting alveoli to the outside air, and elastic properties of the surrounding medium measured by the elastance E. Denoting by $T_{\text{fin}} > 0$ the experiment final time, the time-depending lung volume V and its time derivative $\dot{V}$, which is the corresponding air flow, satisfy, for any $t \in [0, T_{\text{fin}}]$,

$$R\,\dot{V}(t) + E\,(V(t) - \text{FRC}) = -P_{\text{ext}}(t), \tag{1}$$

supplemented with an initial condition on V. In (1), FRC is the functional residual volume (volume at rest) for a healthy patient, $P_{\text{ext}}(t)$ is the muscular pressure leading to the deformation of the lung parenchyma, which induces inspiration (and also, forced expiration) at time t. This last quantity, often referred to as the airway opening or transpulmonary pressure [27, 5], is chosen here as a periodic function, and we denote by $T \in (0, T_{\text{fin}}]$ the corresponding period. Unfortunately, the pressure is not accessible to direct measurements. It accounts for the effort of the diaphragm ($P_{\text{ext}}(t) < 0$ for inspiration), and possibly of the abdomen muscles during a forced expiration ($P_{\text{ext}}(t) = 0$ for passive expiration and $P_{\text{ext}}(t) > 0$ for forced expiration). Note that, for the sake of simplicity, in all the upcoming computations, $t = 0$ corresponds to the beginning of a respiratory cycle, and we set $V(0) = \text{FRC}$. The final time T_{fin} will be chosen as a multiple of T in order to deal with full respiratory cycles.

For the air renewing process, we need to describe the dynamics of both oxygen and carbon dioxide at the alveolar level. In order to do so, we introduce their mole fractions in the alveoli, respectively denoted by χ_{O_2} and χ_{CO_2}. Hence, the proportion of, for instance, oxygen at time t in the alveoli is given by $\chi_{\text{O}_2}(t)[V(t) - V_D]$, where V_D is the lung dead space, *i.e.* the volume of air not involved in the gas exchanges. This dead volume is assumed to be constant during each respiratory cycle, as the sum of the anatomic dead space V_D^A and the extra volume V_D^P depending on the patient state:

$$V_D = V_D^A + V_D^P. \tag{2}$$

The usual value of V_D^A is 0.15 L [34]. We choose to compute the extra pathological dead space for each respiratory cycle $[kT, (k+1)T]$, $k \geq 0$, according to the following formula:

$$V_D^P = \max\left(V(kT) - \text{FRC}, 0\right). \tag{3}$$

This volume measures the discrepancy between a non-pathological functional residual volume FRC and the computed volume at the end of each expiration. This quantity V_D^P is nonnegative, and close to 0 in healthy situations.

The variations of the oxygen and carbon dioxide amounts follow by mass balances, which depend on two fluxes, a transport and a diffusion one.

The first flux describes the transport of each species. At inspiration ($\dot{V}(t) \geq 0$), the alveoli are supplied with fresh air through the bronchial tree. The fluxes are thus expressed as the product of $\dot{V}(t)$ and the corresponding mole fractions entering the alveoli at time t, denoted by $\chi^0_{\text{O}_2}(t)$ and $\chi^0_{\text{CO}_2}(t)$. At expiration ($\dot{V}(t) \leq 0$), the gases are exhaled. Consequently, the fluxes are obtained as the product of $\dot{V}(t)$ and the corresponding mole fractions at time t in the alveoli. During a whole respiratory cycle, the supplied flux of each gas takes the form $\dot{V}(t)\,[\mathbb{1}_{\mathbb{R}_+}(\dot{V}(t))\chi^0(t) + \mathbb{1}_{\mathbb{R}_-}(\dot{V}(t))\,\chi(t)]$.

The second flux takes into account the diffusion phenomena into the blood through the alveolar membrane. We denote by q_{O_2} and q_{CO_2} the corresponding fluxes. They are accurately described in

the next subsection. In particular, the strong coupling between oxygen and carbon dioxide will be further discussed.

To summarize, at each respiratory cycle, the mole fractions of both species in the alveoli satisfy, for any $t \in [kT, (k+1)T]$, $k \geq 0$,

$$\dot{\chi_{\mathrm{O}_2}}(t) = \frac{1}{V(t) - V_D} \left(\dot{V}(t) \left(\chi^0_{\mathrm{O}_2}(t) - \chi_{\mathrm{O}_2}(t) \right) \mathbb{1}_{\mathbb{R}_+}(\dot{V}(t)) - q_{\mathrm{O}_2}(t) \right), \tag{4}$$

$$\dot{\chi_{\mathrm{CO}_2}}(t) = \frac{1}{V(t) - V_D} \left(\dot{V}(t) \left(\chi^0_{\mathrm{CO}_2}(t) - \chi_{\mathrm{CO}_2}(t) \right) \mathbb{1}_{\mathbb{R}_+}(\dot{V}(t)) - q_{\mathrm{CO}_2}(t) \right). \tag{5}$$

The mole fractions $\chi^0_{\mathrm{O}_2}(t)$ and $\chi^0_{\mathrm{CO}_2}(t)$ describe what enters the alveoli during inspiration. It is a mixture of dead-space air, assumed to be filled of gases whose mole fractions are the current ones in the lung, and fresh air, for which $\chi^{\mathrm{atm}}_{\mathrm{O}_2} = 21\%$ and $\chi^{\mathrm{atm}}_{\mathrm{CO}_2} = 0.04\%$. The inspired air volume is given by $V(t) - V(kT)$.We can thus write, for any $t \in [kT, (k+1)T]$,

$$\chi^0_{\mathrm{O}_2}(t) = (1 - \phi(t))\chi^{\mathrm{atm}}_{\mathrm{O}_2} + \phi(t)\chi_{\mathrm{O}_2}(t), \qquad \chi^0_{\mathrm{CO}_2}(t) = (1 - \phi(t))\chi^{\mathrm{atm}}_{\mathrm{CO}_2} + \phi(t)\chi_{\mathrm{CO}_2}(t), \tag{6}$$

where we set

$$\phi(t) = V_D/(V(t) - V(kT) + V_D) > 0. \tag{7}$$

Using (7), (4)–(5) then become

$$\dot{\chi_{\mathrm{O}_2}}(t) = \frac{1}{V(t) - V_D} \left((1 - \phi(t))\, \dot{V}(t) \left(\chi^{\mathrm{atm}}_{\mathrm{O}_2} - \chi_{\mathrm{O}_2}(t) \right) \mathbb{1}_{\mathbb{R}_+}(\dot{V}(t)) - q_{\mathrm{O}_2}(t) \right), \tag{8}$$

$$\dot{\chi_{\mathrm{CO}_2}}(t) = \frac{1}{V(t) - V_D} \left((1 - \phi(t))\, \dot{V}(t) \left(\chi^{\mathrm{atm}}_{\mathrm{CO}_2} - \chi_{\mathrm{CO}_2}(t) \right) \mathbb{1}_{\mathbb{R}_+}(\dot{V}(t)) - q_{\mathrm{CO}_2}(t) \right). \tag{9}$$

We emphasize that, in order for (6) to make sense, we need the quantity $1 - \phi(t)$ to remain non-negative when $\dot{V}(t) \geq 0$ only, and that is the case: during inspiration, V grows and consequently, $V(t) \geq V(kT)$. Besides, note that (8)–(9) differ from their oxygen-only counterpart in [19] since we take the dead space into account: choosing $V_D = 0$ in (8) allows to recover the corresponding equation from [19]. Nevertheless, even for healthy patients, for whom V_D^P is close to zero, taking into account the anatomic dead space, when considering both gases, is crucial to obtain the right order of magnitude of the carbon dioxide quantities, whereas it is not so crucial when considering oxygen alone, as in [19].

Remark 1. *Note that, when the applied external pressure is periodic, there exists a unique periodic solution to* (1)*. This solution is moreover asymptotically stable* [20]*. It implies that, in the periodic regime limit, V_D^P (and thus ϕ) takes the very same value $V_{D_{\mathrm{per}}}^P$ at each respiratory cycle, which can be exactly computed as*

$$V_{D_{\mathrm{per}}}^P = \max\left(-\frac{1}{R(1 - e^{-T/\tau})} \int_0^T e^{-(T-s)/\tau}\, P_{\mathrm{ext}}(s)\, \mathrm{d}s,\, 0 \right).$$

It depends on the parameters of the mechanical model, and in particular on the relaxation time $\tau = R/E$, as well as on the applied external pressure. For instance, it cannot be neglected when the lung resistance R increases or its elastance E decreases.

We now need to properly define the diffusive fluxes q_{O_2} and q_{CO_2}.

2.2. **Modelling of gas exchange and hemoglobin captation.** We assume that the diffusive properties of the blood-gas barrier are constant and uniform along the capillaries. The diffusion process of both gases through the alveolar membrane is a passive diffusion which is thus characterized by two constant diffusion coefficients denoted by D_{m,O_2} and D_{m,CO_2}. It is moreover driven by the difference between the oxygen (resp. carbon dioxide) alveolar pressure $\chi_{\mathrm{O}_2}P_{\mathrm{atm}}$ (resp. $\chi_{\mathrm{CO}_2}P_{\mathrm{atm}}$) and the blood gaseous partial pressure which is denoted by P_{O_2} (resp. P_{CO_2}), where P_{atm} stands for the atmospheric pressure. Recall that the carbon dioxide diffusive capacity is twenty times higher than the oxygen one, see [10, Chapter 39, pp. 493 & 499] for instance.

Next we have to describe the dynamics of binding with hemoglobin. The chemical reaction of each species with hemoglobin is assumed to be instantaneous [10, Chapter 39, p. 499]. As already mentioned, there exists a nonlinear coupling between both gases. In the Haldane effect, the blood oxygenation displaces carbon dioxide from hemoglobin, which increases the removal of carbon dioxide. Consequently, oxygenated blood has a reduced affinity for carbon dioxide and the Haldane effect describes the ability of hemoglobin to carry increased amounts of carbon dioxide in the deoxygenated state as opposed to the oxygenated state. In the Bohr effect, oxygen-binding affinity of hemoglobin is inversely related to both acidity and carbon dioxide concentration. It thus refers to the shift, caused by changes in the carbon dioxide concentration or the environment pH, in the oxygen dissociation curve describing the saturation of hemoglobin with respect to the oxygen partial pressure.

Consequently, the dynamic of the blood partial pressures of oxygen and carbon dioxide can be described through functions representing the concentrations $\mathcal{C}_{\mathrm{O}_2} = \mathcal{C}_{\mathrm{O}_2}(P_{\mathrm{O}_2}, P_{\mathrm{CO}_2})$ and $\mathcal{C}_{\mathrm{CO}_2} = \mathcal{C}_{\mathrm{CO}_2}(P_{\mathrm{O}_2}, P_{\mathrm{CO}_2})$ of O_2 and CO_2 in the blood, which are assumed to be uniform at any time in the whole pulmonary capillary blood volume V_c. The expressions of functions $\mathcal{C}_{\mathrm{O}_2}$ and $\mathcal{C}_{\mathrm{CO}_2}$ are provided later, in Subsections 3.1–3.2.

To define the instantaneous average fluxes $q_{\mathrm{O}_2}(t)$ and $q_{\mathrm{CO}_2}(t)$, let us describe the transfer dynamics, as in [31]: a volume V_c of capillary blood is instantaneously brought in the neighborhood of the alveoli, then remains there during a transient time τ_b, allowing exchanges to take place, and is finally carried away and replaced by the same amount of blood. This phenomenon is periodically reproduced each time period τ_b. Consequently, at every time t, we solve

$$\left\{\begin{array}{rcl} V_c\dfrac{\mathrm{d}}{\mathrm{d}\theta}\left(\mathcal{C}_{\mathrm{O}_2}(P_{\mathrm{O}_2}(t,\theta),P_{\mathrm{CO}_2}(t,\theta))\right) &=& D_{m,\mathrm{O}_2}\left(\chi_{\mathrm{O}_2}(t)P_{\mathrm{atm}}-P_{\mathrm{O}_2}(t,\theta)\right), \\ V_c\dfrac{\mathrm{d}}{\mathrm{d}\theta}\left(\mathcal{C}_{\mathrm{CO}_2}(P_{\mathrm{O}_2}(t,\theta),P_{\mathrm{CO}_2}(t,\theta))\right) &=& D_{m,\mathrm{CO}_2}\left(\chi_{\mathrm{CO}_2}(t)P_{\mathrm{atm}}-P_{\mathrm{CO}_2}(t,\theta)\right), \end{array}\right. \quad \theta\in(0,\tau_b). \tag{10}$$

This system has to be supplemented with initial conditions. Every τ_b, a new quantity of blood arrives, so that it seems fair to choose, at every time t,

$$P_{\mathrm{O}_2}(t,0)=P^v_{\mathrm{O}_2}, \qquad P_{\mathrm{CO}_2}(t,0)=P^v_{\mathrm{CO}_2}, \tag{11}$$

where $P^v_{\mathrm{O}_2}$, $P^v_{\mathrm{CO}_2}$ are the deoxygenated blood pressures of oxygen and carbon dioxide (blood poor in oxygen and rich in carbon dioxide) entering the lung before the gaseous exchanges. We emphasize that t here acts as a parameter, and, at every time t, the above system (10)–(11) must be solved for $\theta\in(0,\tau_b)$.

We are now in a position to properly define the instantaneous average fluxes q_{O_2} and q_{CO_2}. They are determined by the difference between the final blood partial pressure at τ_b and the initial one (which corresponds to the deoxygenated blood) over the transient time τ_b. They are thus written, for any t, as

$$q_{\mathrm{O}_2}(t) = \frac{V_c}{\tau_b}\left(\mathcal{C}_{\mathrm{O}_2}(P_{\mathrm{O}_2}(t,\tau_b),P_{\mathrm{CO}_2}(t,\tau_b))-\mathcal{C}_{\mathrm{O}_2}(P^v_{\mathrm{O}_2},P^v_{\mathrm{CO}_2})\right), \tag{12}$$

$$q_{\mathrm{CO}_2}(t) = \frac{V_c}{\tau_b}\left(\mathcal{C}_{\mathrm{CO}_2}(P_{\mathrm{O}_2}(t,\tau_b),P_{\mathrm{CO}_2}(t,\tau_b))-\mathcal{C}_{\mathrm{CO}_2}(P^v_{\mathrm{O}_2},P^v_{\mathrm{CO}_2})\right). \tag{13}$$

Note that, in this model, $P_{\mathrm{O}_2}(t,\tau_b)$ and $P_{\mathrm{CO}_2}(t,\tau_b)$ represent the instantaneous oxygenated blood pressures at time t and thus are the surrogates of the arterial blood pressures. They hence will be denoted, from now on, by $P^a_{\mathrm{O}_2}(t)$ and $P^a_{\mathrm{CO}_2}(t)$, respectively.

The exchange dynamics at the alveolar-capillary interface leads to the following situations:

- $P^a_{\mathrm{O}_2}(t) \simeq \chi_{\mathrm{O}_2}(t)P_{\mathrm{atm}}$, $P^a_{\mathrm{CO}_2}(t) \simeq \chi_{\mathrm{CO}_2}(t)P_{\mathrm{atm}}$ in healthy situations (for which equilibrium between the alveolar partial pressures and the blood partial pressures is reached for both gases during the transient time);
- if kinetic limitation occurs, $P^a_{\mathrm{O}_2}(t) < \chi_{\mathrm{O}_2}(t)P_{\mathrm{atm}}$ (same for CO_2), and the equilibrium is not reached during the transient time, which can happen for several pathologies.

Yet, in both cases, the corresponding O_2 and CO_2 transfer rates are given by (12)–(13).

2.3. **Full 0D model.** As a consequence, the mechanical and gas exchange model describing the evolution of the lung is written as a nonlinear first-order differential system governing the behaviour of three observable quantities ($t \mapsto V(t)$, $t \mapsto \chi_{\mathrm{O}_2}(t)$ and $t \mapsto \chi_{\mathrm{CO}_2}(t)$), which also requires to compute q_{O_2}, q_{CO_2} and auxiliary quantities $P^a_{\mathrm{O}_2}$, $P^a_{\mathrm{CO}_2}$, at each time t. Let us rewrite the whole dynamical system which we consider, *i.e.* Eqns. (1)–(3) and (7)–(13),

Mechanical model

$$\dot V(t) = -\frac{1}{\tau}(V(t) - \mathrm{FRC}) + \frac{1}{R}P_{\mathrm{ext}}(t), \qquad \text{where } \tau = \frac{R}{E}$$

Balance of gases in the lung volume during each respiratory cycle $[kT, (k+1)T]$

$$\dot{\chi_{\mathrm{O}_2}}(t) = \frac{1}{V(t) - V_D}\left[(1-\phi(t))\,\dot V\,(\chi^{\mathrm{atm}}_{\mathrm{O}_2}(t) - \chi_{\mathrm{O}_2}(t))\,\mathbb{1}_{\mathbb{R}_+}(\dot V(t)) - q_{\mathrm{O}_2}(t)\right]$$

$$\dot{\chi_{\mathrm{CO}_2}}(t) = \frac{1}{V(t) - V_D}\left[(1-\phi(t))\,\dot V\,(\chi^{\mathrm{atm}}_{\mathrm{CO}_2}(t) - \chi_{\mathrm{CO}_2}(t))\,\mathbb{1}_{\mathbb{R}_+}(\dot V(t)) - q_{\mathrm{CO}_2}(t)\right]$$

$$\text{where } V_D = V_D^A + \max(V(kT) - \mathrm{FRC}, 0) \text{ and } \phi(t) = V_D/\left(V(t) - V(kT) + V_D\right)$$

Instantaneous gas fluxes through the alveolo-capillary membrane

$$q_{\mathrm{O}_2}(t) = \frac{V_c}{\tau_b}\left(\mathcal{C}_{\mathrm{O}_2}(P^a_{\mathrm{O}_2}(t), P^a_{\mathrm{CO}_2}(t)) - \mathcal{C}_{\mathrm{O}_2}(P^v_{\mathrm{O}_2}, P^v_{\mathrm{CO}_2})\right)$$

$$q_{\mathrm{CO}_2}(t) = \frac{V_c}{\tau_b}\left(\mathcal{C}_{\mathrm{CO}_2}(P^a_{\mathrm{O}_2}(t), P^a_{\mathrm{CO}_2}(t)) - \mathcal{C}_{\mathrm{CO}_2}(P^v_{\mathrm{O}_2}, P^v_{\mathrm{CO}_2})\right)$$

Instantaneous partial pressures in arterial blood

$(P^a_{\mathrm{O}_2}(t), P^a_{\mathrm{CO}_2}(t)) = (P_{\mathrm{O}_2}(t,\tau_b), P_{\mathrm{CO}_2}(t,\tau_b))$, where $\theta \mapsto (P_{\mathrm{O}_2}(t,\theta), P_{\mathrm{CO}_2}(t,\theta))$ solves

$$\begin{cases}
V_c\dfrac{\mathrm{d}}{\mathrm{d}\theta}\left(\mathcal{C}_{\mathrm{O}_2}(P_{\mathrm{O}_2}(t,\theta), P_{\mathrm{CO}_2}(t,\theta))\right) &=& D_{m,\mathrm{O}_2}\left(\chi_{\mathrm{O}_2}(t)P_{\mathrm{atm}} - P_{\mathrm{O}_2}(t,\theta)\right), & \theta \in (0,\tau_b)\\
V_c\dfrac{\mathrm{d}}{\mathrm{d}\theta}\left(\mathcal{C}_{\mathrm{CO}_2}(P_{\mathrm{O}_2}(t,\theta), P_{\mathrm{CO}_2}(t,\theta))\right) &=& D_{m,\mathrm{CO}_2}\left(\chi_{\mathrm{CO}_2}(t)P_{\mathrm{atm}} - P_{\mathrm{CO}_2}(t,\theta)\right), & \theta \in (0,\tau_b)\\
P_{\mathrm{O}_2}(t,0) &=& P^v_{\mathrm{O}_2}, &\\
P_{\mathrm{CO}_2}(t,0) &=& P^v_{\mathrm{CO}_2}. &
\end{cases}$$

This system has to be supplemented with initial conditions on V, χ_{O_2} and χ_{CO_2}, and the functions $\mathcal{C}_{\mathrm{O}_2}$ and $\mathcal{C}_{\mathrm{CO}_2}$ are defined below, see (18) and (21). As already stated, the determination of instantaneous partial pressures in arterial blood requires to solve the last system at each time step.

Furthermore, the system is completely driven by the muscle command $t \mapsto P_{\mathrm{ext}}(t)$. The parameters, which could be fitted to model pathologies, are the resistance of the bronchial tree (that may be increased, for instance, to model asthma), the elastance of the lung parenchyma (that could be changed in fibrosis or emphysema modelling), the diffusion parameters (that could be decreased in infectious diseases). The parameters R and E have a direct impact on the ventilation process (and

thus on the dynamic of lung volume and available fresh air) whereas the parameters D_m play a crucial role in the gas diffusion. Note that V_c and τ_b are two other constants which can be fitted to take into account some haemodynamic changes.

Remark 2. *From the numerical viewpoint, it is useful to notice that System* (10) *can be formally written as*

$$\left\{\begin{array}{rcl} \dfrac{\mathrm{d}}{\mathrm{d}t}\left(F(u,v)\right) & = & f(u), \\ \dfrac{\mathrm{d}}{\mathrm{d}t}\left(G(u,v)\right) & = & g(v), \end{array}\right.$$

with initial data for u and v. Thus we get

$$\left\{\begin{array}{rcl} \partial_u F(u,v)\dot{u} + \partial_v F(u,v)\dot{v} & = & f(u), \\ \partial_u G(u,v)\dot{u} + \partial_v G(u,v)\dot{v} & = & g(v), \end{array}\right.$$

so that

$$\left\{\begin{array}{rcl} \dot{u} & = & \dfrac{\partial_v G(u,v) f(u) - \partial_v F(u,v) g(u)}{\partial_u F(u,v)\partial_v G(u,v) - \partial_v F(u,v)\partial_u G(u,v)}, \\ \dot{v} & = & -\dfrac{\partial_u G(u,v) f(u) - \partial_u F(u,v) g(u)}{\partial_u F(u,v)\partial_v G(u,v) - \partial_v F(u,v)\partial_u G(u,v)}, \end{array}\right.$$

if the denominator is non-zero. It will be the case for the parameter ranges and the functions F and G which we shall deal with.

3. Gas exchange model for oxygen and carbon dioxide

In this section, we focus on the coupled diffusion process involving oxygen and carbon dioxide through the so-called Bohr and Haldane effects, in order to define the functions $\mathcal{C}_{\mathrm{O}_2}$, $\mathcal{C}_{\mathrm{CO}_2}$.

3.1. Balance of oxygen including the Bohr effect.

In order to describe the oxygen concentration in the blood and take into account the Bohr effect, we adapt the model developped in [19, Sn. 2] by including the dependency of the O_2 saturation with respect to CO_2.

Classically, the oxygen concentration in blood plasma can be expressed in terms of the oxygen partial pressure, as σP_{O_2}, where $\sigma = 1.4{\cdot}10^{-6}\,\mathrm{mol}{\cdot}\mathrm{L}^{-1}{\cdot}\mathrm{mmHg}^{-1}$ denotes the oxygen solubility in the plasma. To this oxygen concentration in plasma, one must add a significant contribution due to the capture of some O_2 by hemoglobin (Hb). This latter contribution is written as $4C_{\mathrm{Hb}}\mathcal{H}_0(P_{\mathrm{O}_2})$, where C_{Hb} is the total concentration of hemoglobin (in both native and combined forms), $\mathcal{H}_0 : \mathbb{R}_+ \to [0,1]$ allows to quantify the hemoglobin saturation, and 4 is the maximal number of oxygen molecules that a hemoglobin molecule may carry. This saturation function $\mathcal{H}_0$ [14, 34] is often referred to as *Hill's* or *oxygen dissociation curve*, and can be expressed as

$$\mathcal{H}_0(P_{\mathrm{O}_2}) = \frac{{P_{\mathrm{O}_2}}^{2.5}}{{P_0}^{2.5} + {P_{\mathrm{O}_2}}^{2.5}}, \tag{14}$$

where $P_0 = 26\,\mathrm{mmHg}$, see [14] and Figure 1. The oxygen concentration in the blood in both forms (free and captured by hemoglobin) is then written as

$$\mathcal{C}_{\mathrm{O}_2}(P_{\mathrm{O}_2}) = \sigma P_{\mathrm{O}_2} + 4C_{\mathrm{Hb}}\mathcal{H}_0(P_{\mathrm{O}_2}). \tag{15}$$

That simple model allows to recover, without tuning up any parameter, the order of magnitude of the oxygen transfer rate at rest [10, 32, 33] for healthy situations, namely $q_{\mathrm{O}_2} = 250\,\mathrm{mL}\cdot\mathrm{min}^{-1}$, see [19].

Nevertheless, the Bohr effect is still not taken into account in (15), since the expression of $\mathcal{C}_{\mathrm{O}_2}$ does not depend on P_{CO_2}. In fact, the oxygen dissociation curve, and hence the total concentration of oxygen in the blood, depend on several factors, such as pH, P_{CO_2}, temperature, *etc.* Here, we

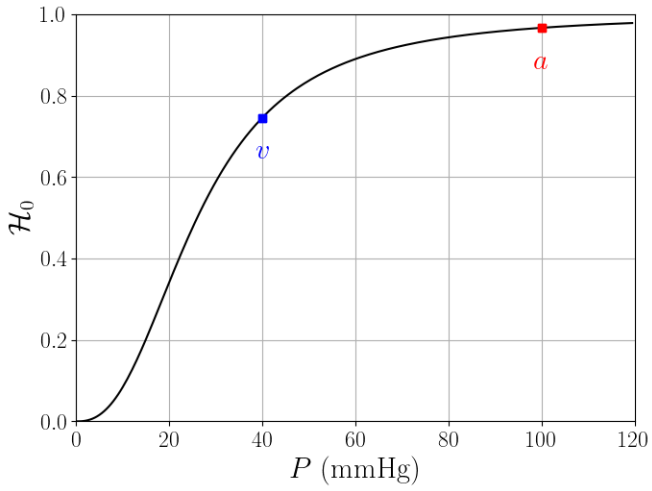

FIGURE 1. Oxygen dissociation curve: in standard conditions, venous blood is poor in oxygen ($P^v_{O_2} = 40$ mmHg, corresponding to Hb saturation at 75%) whereas arterial blood has been enriched in O_2, through the diffusion process during the travel in the capillary ($P^a_{O_2} = 100$ mmHg, corresponding to Hb saturation at 97.5%).

choose to include in our model not only the influence of P_{CO_2}, but also the one of pH, and to neglect the temperature influence: we replace the classical Hill curve $\mathcal{H}_0$ by

$$P_{O_2} \mapsto \mathcal{H}(P_{O_2}, P_{CO_2}, \text{pH}).$$

The expression of $\mathcal{H}(P_{O_2}, P_{CO_2}, \text{pH})$ can be built by considering the following modification, proposed in [15]:

$$\mathcal{H}(P_{O_2}, P_{CO_2}, \text{pH}) = \mathcal{H}_0\left(\mathcal{P}(P_{O_2}, P_{CO_2}, \text{pH})\right) \tag{16}$$

$$\mathcal{P}(P_{O_2}, P_{CO_2}, \text{pH}) = P_{O_2} \cdot 10^{0.40\cdot(\text{pH}-7.4)+0.06\cdot(\log_{10}(40)-\log_{10}(P_{CO_2}))}. \tag{17}$$

Here, (17) includes a correction factor which accounts for the variations of pH and P_{CO_2} and their distances to their reference values in healthy situations, namely 7.4 for the average blood pH, and 40 mmHg for the standard average carbon dioxide arterial blood partial pressure. Hence, the new expression of $\mathcal{C}_{O_2}$ is given by

$$\begin{aligned}\mathcal{C}_{O_2}(P_{O_2}, P_{CO_2}, \text{pH}) &= \sigma P_{O_2} + 4C_{\text{Hb}}\ \mathcal{H}(P_{O_2}, P_{CO_2}, \text{pH}) \\ &= \sigma P_{O_2} + 4C_{\text{Hb}}\ \mathcal{H}_0\left(P_{O_2} \cdot 10^{0.40\cdot(\text{pH}-7.4)+0.06\cdot(\log_{10}(40)-\log_{10}(P_{CO_2}))}\right),\end{aligned} \tag{18}$$

where $\mathcal{H}_0$ is the standard Hill curve defined by (14).

Remark 3. *One can also eliminate* pH *as a given parameter and take into account the acid-base equilibrium. The study of the acid-base* CO_2/HCO_3^- *is described in* [34, Chap. 6, pp. 96–101] *and leads to*

$$\text{pH} = \text{p}K_A + \log_{10}\frac{C_{HCO_3^-}}{0.03 \cdot P_{CO_2}}, \tag{19}$$

where $\text{p}K_A = 6.1$ *is the dissociation constant of carbonic acid and* $C_{HCO_3^-}$ *denotes the bicarbonate concentration in the blood, expressed in* $\text{mmol}\cdot\text{L}^{-1}$*. This concentration is mainly regulated by the kidney and its normal value lies between* $22\,\text{mmol}\cdot\text{L}^{-1}$ *and* $26\,\text{mmol}\cdot\text{L}^{-1}$*. The normal bicarbonate concentration in the arterial blood is around* $24\,\text{mmol}\cdot\text{L}^{-1}$*, whereas it is* $26\,\text{mmol}\cdot\text{L}^{-1}$ *for venous blood. It means in particular that, first, the default value of* pH *in the arterial blood is* 7.4 *as expected*

and, second, as long as the ratio between $C_{\mathrm{HCO}_3^-}$ *and* $0.03 \cdot P_{\mathrm{CO}_2}$ *equals* 20*, the value of* pH *remains at* 7.4.

In this case, the expression of the oxygen concentration with respect to the partial pressures of oxygen and carbon dioxide would be given by

$$\tilde{\mathcal{C}}_{\mathrm{O}_2}(P_{\mathrm{O}_2}, P_{\mathrm{CO}_2}, C_{\mathrm{HCO}_3^-}) = \sigma P_{\mathrm{O}_2} + 4C_{\mathrm{Hb}}\mathcal{H}\left(P_{\mathrm{O}_2}, P_{\mathrm{CO}_2}, 6.10 + \log_{10}\frac{C_{\mathrm{HCO}_3^-}}{0.03 \cdot P_{\mathrm{CO}_2}}\right), \tag{20}$$

where $\mathcal{H}$ *is defined by* (16).

In the next paragraphs, we study the influence of pH and P_{CO_2} on the oxygen dissociation curves.

Influence of pH *for a fixed value of* P_{CO_2}. On Figure 2a, the function $P_{\mathrm{O}_2} \mapsto \mathcal{H}(P_{\mathrm{O}_2}, P_{\mathrm{CO}_2}, \mathrm{pH})$ is plotted for $P_{\mathrm{CO}_2} = 40\,\mathrm{mmHg}$ (arterial blood pressure in a healthy regime) and different values of pH (including extremal ones which do not correspond to standard physiological regimes). Note that the profile of $P_{\mathrm{O}_2} \mapsto \mathcal{H}(P_{\mathrm{O}_2}, P_{\mathrm{CO}_2}, \mathrm{pH})$ for $P_{\mathrm{CO}_2} = 46\,\mathrm{mmHg}$ (venous blood pressure in a healthy regime) is roughly identical. Actually, only little difference is observed when P_{CO_2} is set in the whole interval $(5, 80)$. Consequently, for a fixed value of P_{CO_2}, the chosen oxygen dissociation curve is not very sensitive to pH.

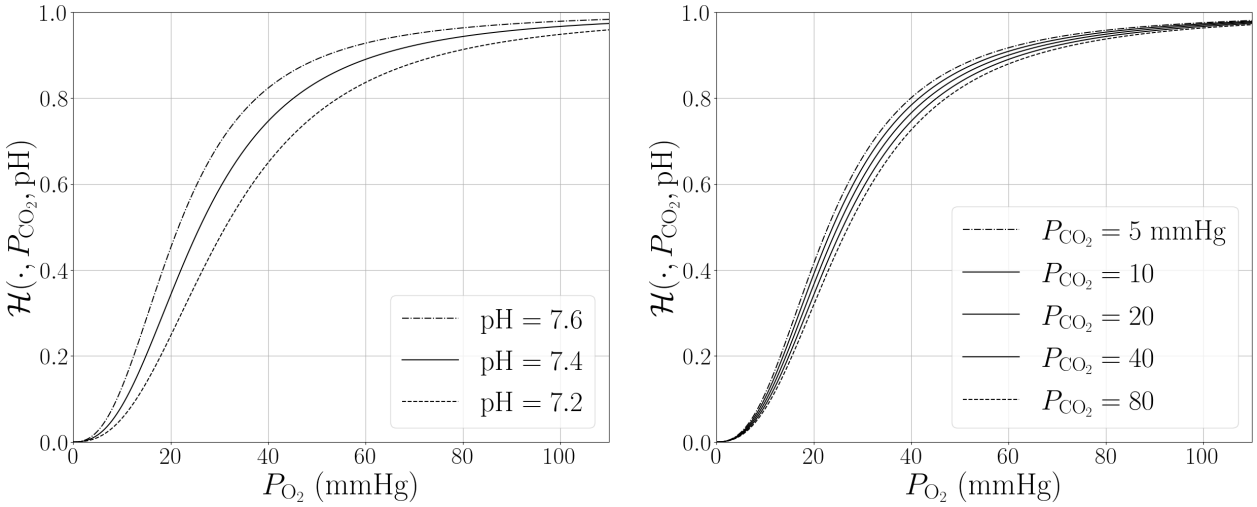

FIGURE 2. Oxygen dissociation curves $P_{\mathrm{O}_2} \mapsto \mathcal{H}(P_{\mathrm{O}_2}, P_{\mathrm{CO}_2}, \mathrm{pH})$ for (a) $P_{\mathrm{CO}_2} = 40\,\mathrm{mmHg}$ and various pH, and (b) $\mathrm{pH} = 7.4$ and various values of P_{CO_2}.

Influence of P_{CO_2} *for a fixed value of* pH. The function $P_{\mathrm{O}_2} \mapsto \mathcal{H}(P_{\mathrm{O}_2}, P_{\mathrm{CO}_2}, \mathrm{pH})$ is described for $\mathrm{pH} = 7.4$ on Figure 2b. We observe that the oxygen dissociation curve is not deeply impacted by the variations of P_{CO_2}. The sensitivity of the curve with respect to P_{CO_2} is really low.

3.2. **Balance of carbon dioxide including the Haldane effect.** The carbon dioxide concentration in the blood is determined by its different forms, as CO_2 is carried in the blood in three forms: dissolved, after a chemical reaction, that implies hemoglobin, as bicarbonate, and in combination with proteins as carbamino compounds. The major quantity of carbon dioxide reacts with hemoglobin which fixes H^+ ions and leads to the bicarbonate creation. This binding gives rise to the Haldane effect, where blood deoxygenation increases its ability to carry H^+, see [34]: the presence of reduced hemoglobin in the peripheral blood helps with the CO_2 loading, whereas the oxygenation occurring in the pulmonary capillary supports the unloading. The relationship between the partial

pressure of CO_2 and the total CO_2 concentration in the blood (in all forms) is often referred to as the carbon dioxide dissociation curve, and it is much more linear than is the oxygen dissociation curve, at least in standard regimes.

Actually, as pointed out e.g. in [34], because of the Haldane effect, the exchange dynamics of CO_2 is strongly influenced by the dynamics of O_2, as oxygenated blood carries less carbon dioxide for the same oxygen partial pressure. In terms of mathematical modelling, it means that the function $\mathcal{C}_{CO_2}$, which models the concentration of CO_2 in the blood in all forms, highly depends on the partial pressure of O_2. Several phenomenological formulas have been proposed in the literature to account for this phenomenon, see [17, 18] for instance. We choose to use here, for the sake of simplicity, the Meade formula [21], giving the concentration in $\text{mol} \cdot \text{L}^{-1}$

$$\mathcal{C}_{CO_2}(P_{O_2}, P_{CO_2}) = \frac{10^{-3}}{V_m}\left(463\, e^{0.00415 P_{CO_2}} - 340\, e^{-0.0445 P_{CO_2}} + 62(0.975 - \mathcal{H}_0(P_{O_2}))\right), \tag{21}$$

where $\mathcal{H}_0$ is the oxygen Hill function defined by (14) and V_m the molar volume of an ideal gas at standard temperature and pressure, namely $V_m = 22.4\ \text{L} \cdot \text{mol}^{-1}$. The dependence with respect to pH is not taken into account. Note that this fitted formula may not be the most accurate but it illustrates the Haldane effect and the strong coupling between O_2 and CO_2.

Figure 3 represents the function $P_{CO_2} \mapsto \mathcal{C}_{CO_2}(P_{O_2}, P_{CO_2})$ for two values of P_{O_2}, namely 40 and 100 mmHg, corresponding to venous and arterial oxygen partial pressures in healthy situations.

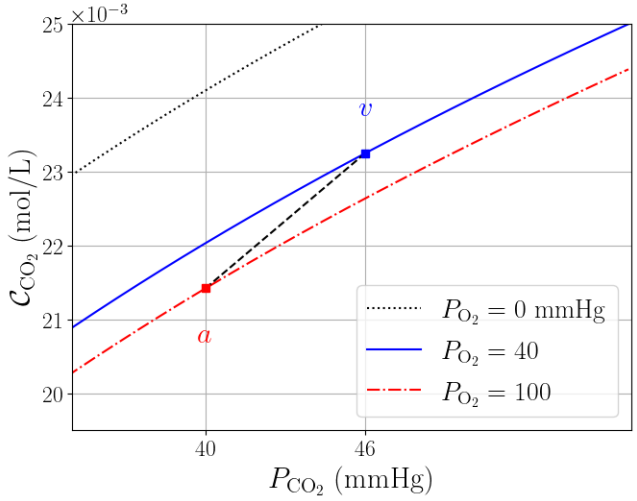

FIGURE 3. Carbon dioxide dissociation curve $P_{CO_2} \mapsto \mathcal{C}_{CO_2}(P_{O_2}, P_{CO_2})$.

3.3. **Quantitative study of the coupled diffusion process.** Thanks to (18) for the oxygen concentration with Bohr's effect, and (21) for the carbon dioxide concentration with Haldane's, we can estimate the neat transfer rate for both O_2 and CO_2. We consider the following standard values for the venous and arterial pressures

$$\begin{aligned} P^v_{O_2} &= 40\,\text{mmHg}, & P^v_{CO_2} &= 46\,\text{mmHg}, \\ P^a_{O_2} &= 100\,\text{mmHg}, & P^a_{CO_2} &= 40\,\text{mmHg}. \end{aligned} \tag{22}$$

Based on (18) and Table 16 from Appendix A, the oxygen transfer rate can be estimated by

$$q_{O_2} = \frac{V_c}{\tau_b}\left(\mathcal{C}_{O_2}(P^a_{O_2}, P^a_{CO_2}, 7.4) - \mathcal{C}_{O_2}(P^v_{O_2}, P^v_{CO_2}, 7.4)\right) = 1.92 \cdot 10^{-4}\ \text{mol} \cdot \text{s}^{-1},$$

or, involving the molar volume V_m of an ideal gas, we get

$$q_{O_2} = 258\ \text{mL} \cdot \text{min}^{-1}.$$

We can also estimate the transfer rate of CO_2, based on (21), as

$$q_{\mathrm{CO}_2} = \frac{V_c}{\tau_b}\left(\mathcal{C}_{\mathrm{CO}_2}(P^a_{\mathrm{O}_2}, P^a_{\mathrm{CO}_2}) - \mathcal{C}_{\mathrm{CO}_2}(P^v_{\mathrm{O}_2}, P^v_{\mathrm{CO}_2})\right) = -1.70 \cdot 10^{-4}\ \mathrm{mol}\cdot\mathrm{s}^{-1},$$

or, using again V_m,

$$q_{\mathrm{CO}_2} = -228\ \mathrm{mL}\cdot\mathrm{min}^{-1}.$$

The standard values of the fluxes are respectively around $250\ \mathrm{mL}\cdot\mathrm{min}^{-1}$ for the oxygen, and around $-200\ \mathrm{mL}\cdot\mathrm{min}^{-1}$ for the carbon dioxide. We observe that, compared to those standard values, the computations from (18) and (21) give the same order of magnitude. Moreover, note that if we compute the associated respiratory quotient, denoted by RQ and defined as $|q_{\mathrm{CO}_2}/q_{\mathrm{O}_2}|$, we obtain $\mathrm{RQ} = 0.884$, which also lies in the standard range for this ratio.

Remark 4. *At rest, the Bohr and Haldane effects do not seem to have the same importance in healthy regimes (with* $(P^v_{\mathrm{O}_2}, P^v_{\mathrm{CO}_2}) = (40, 46)$ *and* $(P^a_{\mathrm{O}_2}, P^a_{\mathrm{CO}_2}) = (100, 40)$*, all values given in* mmHg*), see* [11, 9, 10, 18]*. In the static regime, neglecting the Haldane effect produces a sharp reduction of the carbon dioxide flux (*-37%*), whereas the Bohr effect seems totally negligible, since it has no effect of the oxygen flux.*

Remark 5. *When taking into account the bicarbonate concentration instead of* pH*, based on* (20)*, remembering that* $C_{\mathrm{HCO}_3^-} = 24\ \mathrm{mmol}\cdot\mathrm{L}^{-1}$*, we obtain*

$$q_{\mathrm{O}_2} = \frac{V_c}{\tau_b}\left(\tilde{\mathcal{C}}_{\mathrm{O}_2}(P^a_{\mathrm{O}_2}, P^a_{\mathrm{CO}_2}, 24) - \tilde{\mathcal{C}}_{\mathrm{O}_2}(P^v_{\mathrm{O}_2}, P^v_{\mathrm{CO}_2}, 24)\right) = 2.15 \cdot 10^{-4}\ \mathrm{mol}\cdot\mathrm{s}^{-1},$$

or, using V_m*,*

$$q_{\mathrm{O}_2} = 289\ \mathrm{mL}\cdot\mathrm{min}^{-1}.$$

The associated respiratory quotient is then $\mathrm{RQ} = 0.789$*, which remains in the standard range.*

Let us now investigate the possible diffusion limitation by solving a dynamical system, similar to (10), satisfied by the oxygen and carbon dioxide blood pressures, for different values of the diffusion coefficients. This system is written as

$$\left\{\begin{array}{rcll} V_c\dfrac{\mathrm{d}}{\mathrm{d}\theta}\left(\mathcal{C}_{\mathrm{O}_2}(P_{\mathrm{O}_2}, P_{\mathrm{CO}_2}, \mathrm{pH})\right) &=& D_{m,\mathrm{O}_2}\left(P^{\mathrm{alv}}_{\mathrm{O}_2} - P_{\mathrm{O}_2}\right), & \theta \in (0, \tau_b), \\ V_c\dfrac{\mathrm{d}}{\mathrm{d}\theta}\left(\mathcal{C}_{\mathrm{CO}_2}(P_{\mathrm{O}_2}, P_{\mathrm{CO}_2})\right) &=& D_{m,\mathrm{CO}_2}\left(P^{\mathrm{alv}}_{\mathrm{CO}_2} - P_{\mathrm{CO}_2}\right), & \theta \in (0, \tau_b), \\ P_{\mathrm{O}_2}(0) &=& P^v_{\mathrm{O}_2}, & \\ P_{\mathrm{CO}_2}(0) &=& P^v_{\mathrm{CO}_2}, & \end{array}\right. \tag{23}$$

where $P^{\mathrm{alv}}_{\mathrm{O}_2}$ and $P^{\mathrm{alv}}_{\mathrm{CO}_2}$ are the gas partial pressures in the alveolar compartment, and pH is set at 7.4. We define the following reference situation:

- the gas partial pressures in the venous blood are chosen as in (22);
- the gas partial pressures in the alveolar compartment are chosen equal to the arterial reference values given in (22);
- the membrane is healthy, e.g.

$$D^{\mathrm{h}}_{m,\mathrm{O}_2} = 21\,\mathrm{mL}\cdot\mathrm{min}^{-1}\cdot\mathrm{mmHg}^{-1},$$
$$D^{\mathrm{h}}_{m,\mathrm{CO}_2} = 20 D^{\mathrm{h}}_{m,\mathrm{O}_2} = 420\,\mathrm{mL}\cdot\mathrm{min}^{-1}\cdot\mathrm{mmHg}^{-1}.$$

We then investigate three different values of the diffusion coefficients: $D_m = D^{\mathrm{h}}_m$, $D_m = D^{\mathrm{h}}_m/2$ and $D_m = D^{\mathrm{h}}_m/4$, D_{m,CO_2} remaining equal to $20 D_{m,\mathrm{O}_2}$. The other parameters are set to their reference values, see Table 16.

The time evolution of the partial pressures of both gases on Figure 4 illustrates the kinetic limitation phenomenon. It allows to highlight several observations.

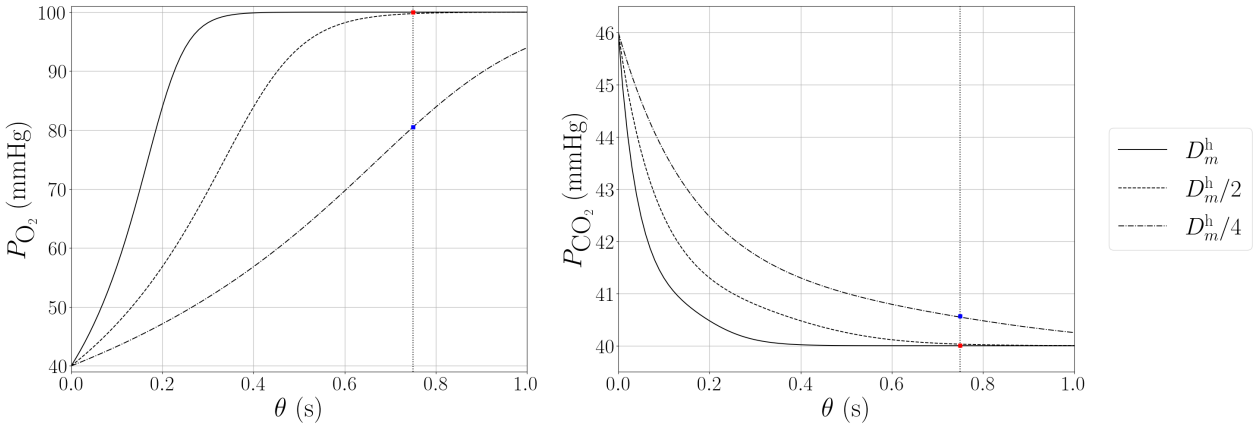

FIGURE 4. Dynamics of the gas exchange through the alveolo-capillary membrane: $\theta \mapsto P_{O_2}(\theta)$ and $\theta \mapsto P_{CO_2}(\theta)$.

First, in the reference healthy regime, partial pressures evolve from the venous (or deoxygenated) value to the alveolar one. Equilibrium is reached within the available time $\tau_b = 0.75$ s and it has some robustness since the time needed to obtain this balance is about the third of τ_b.
Second, in a moderately impaired regime, e.g. $D_m = D_m^h/2$ for both species, we observe that the equilibrium between partial pressures is reached around time τ_b, *i.e.*

$$P^a_{O_2} \simeq P^{alv}_{O_2}, \qquad P^a_{CO_2} \simeq P^{alv}_{CO_2},$$

even if the gas exchange dynamics has been slowed down by the membrane impairment. This impairment is not sufficient to deteriorate the gas transfer: q_{O_2} and q_{CO_2} have the same values as in the healthy case.
Eventually, in a severely impaired regime, e.g. $D_m = D_m^h/4$ for both gases, we observe that the equilibrium between partial pressures is not reached. As a consequence, we have

$$P^a_{O_2} < P^{alv}_{O_2}, \qquad P^a_{CO_2} > P^{alv}_{CO_2},$$

and the neat transfer of gases, for both O_2 and CO_2, is lowered, compared to the healthy situation.

In the above example, possible kinetic limitation has been illustrated by considering different values of the diffusing membrane. Note that the kinetic limitation may also occur in other situations: if τ_b is significantly reduced and V_c is increased (e.g. during exercise), it may drop below the time necessary to achieve equilibrium between the partial pressures.

In the following sections, we present various numerical studies. We start by illustrating our model behaviour for a healthy patient in two cases: standard respiration and hyperventilation. Starting from this reference situation, we investigate the model sensitivity, with respect to the physical parameters of resistance, elastance and diffusion coefficients of the alveolo-capillary membrane, of two types of characteristic ouputs, the alveolo-capillary fluxes and the oxygenated blood partial pressures. More precisely, we explore whether there exist global structures in the input parameters and study their crossed sensitivity. Eventually, we try to recover known qualitative behaviours by varying the various physical parameters to mimick pathological situations such as asthma, emphysema...

4. Healthy reference respiration scenarios

We first investigate a healthy situation within a normal respiration framework. The mechanical parameters are set as

$$R^{\mathrm{h}} = 2\ \mathrm{cmH_2O}\cdot\mathrm{L}^{-1}\cdot\mathrm{s}, \qquad E^{\mathrm{h}} = 3.5\ \mathrm{cmH_2O}\cdot\mathrm{L}^{-1}, \tag{24}$$

so that the relaxation time $\tau^{\mathrm{h}} = R^{\mathrm{h}}/E^{\mathrm{h}}$ associated to the mechanical model (1) equals 0.57 s. For the dead space volume in (2), we recall the standard value of the anatomical dead space for a healthy man $V_D^A = 0.15$ L. For the diffusive model (10), we choose the same healthy values as in the previous section, which are

$$D^{\mathrm{h}}_{m,\mathrm{O_2}} = 21\,\mathrm{mL}\cdot\mathrm{min}^{-1}\cdot\mathrm{mmHg}^{-1} = 1.6\cdot10^{-5}\,\mathrm{mol}\cdot\mathrm{s}^{-1}\cdot\mathrm{mmHg}^{-1}, \tag{25}$$

$$D^{\mathrm{h}}_{m,\mathrm{CO_2}} = 20D^{\mathrm{h}}_{m,\mathrm{O_2}} = 420\,\mathrm{mL}\cdot\mathrm{min}^{-1}\cdot\mathrm{mmHg}^{-1} = 3.2\cdot10^{-4}\,\mathrm{mol}\cdot\mathrm{s}^{-1}\cdot\mathrm{mmHg}^{-1}. \tag{26}$$

We impose a periodic breathing scenario where the period T equals 5 s. The applied pressure P_{ext} is chosen piecewise constant, namely, in mmHg, such that

$$P_{\mathrm{ext}}(t) = -2, \quad 0 \le t < i_{\mathrm{frac}}T, \qquad P_{\mathrm{ext}}(t) = 0, \quad i_{\mathrm{frac}}T \le t < T, \tag{27}$$

where the inspiration proportion i_{frac} is set to 0.35. In all the following tables, we listed averaged quantities over a time period, denoted by $\langle\,\cdot\,\rangle$, while making sure periodic behaviour is approximately reached (more precisely, average over the last period for a final time $T_{\mathrm{fin}} = 50$ s). First, in this healthy situation, one can check that the values from Table 1 are standardly acknowledged.

Table 1. Averaged quantities in the healthy case with standard breathing parameters.

$\langle q_{\mathrm{O_2}}\rangle$ (mL/min)	$\langle q_{\mathrm{CO_2}}\rangle$ (mL/min)	RQ –	$\langle P^a_{\mathrm{O_2}}\rangle$ (mmHg)	$\langle P^a_{\mathrm{CO_2}}\rangle$ (mmHg)	$\langle \chi_{\mathrm{O_2}}\rangle$ –	$\langle \chi_{\mathrm{CO_2}}\rangle$ –	V_D (L)	$V_{\min}$ (L)	$V_{\max}$ (L)
256	−203	0.793	97.6	41	13.7%	5.74%	0.152	2.50	3.05

Moreover, our quantities of interest evolve with respect to time as shown in Figures 5–7.

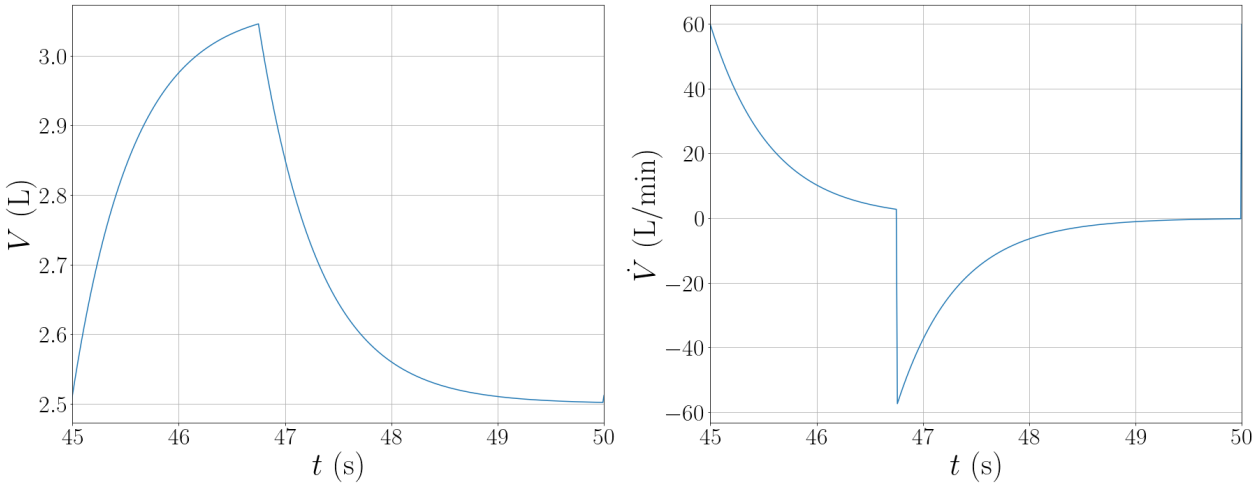

Figure 5. Plots w.r.t. time of (a) the total volume V and (b) the air flow $\dot{V}$.

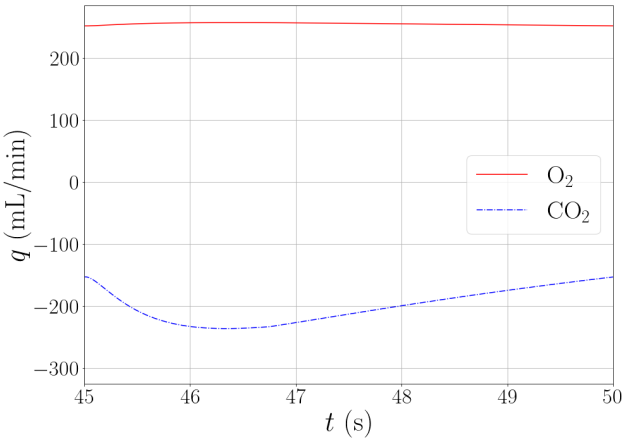

FIGURE 6. Plot w.r.t. time of the gaseous fluxes q_{O_2} and q_{CO_2}.

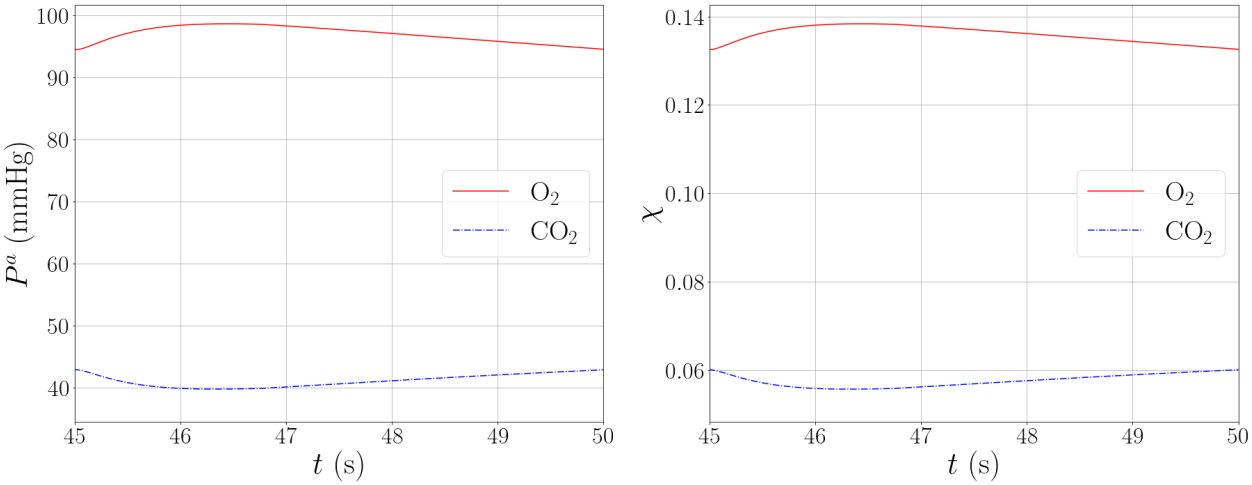

FIGURE 7. Plots w.r.t. time of (a) the arterial (or oxygenated) blood pressures $P^a_{O_2}$, $P^a_{CO_2}$, and (b) the alveolar mole fractions χ_{O_2}, χ_{CO_2}.

Remark 6. *Note that, in this healthy situation, the extra pathological dead space V_D^P is negligible and the volume at the end of expiration almost equals* FRC. *Moreover, taking the anatomical dead space into account appears as crucial to recover the correct orders of magnitude of the physiological quantities. Indeed, when imposing $V_D = 0$, and subsequently $\phi = 0$ instead of* (7)*, we obtain the gas exchange values given in Table 2, the dynamics of the lung respiratory volume remaining unchanged. In particular, compared to Table 1, the impact of the dead space volume is especially clear for the carbon dioxide flux and arterial pressure.*

We can also consider a hyperventilation scenario for a healthy patient, by choosing $T = 2$ s (instead of 5) and $i_{\text{frac}} = 0.5$ (instead of 0.35).

We can then observe changes for carbon dioxide quantities in Table 3, compared to Table 1: the absolute value of the carbon dioxide flux significantly increases, whereas the oxygen one remains

TABLE 2. Averaged gas quantities in the healthy case with $V_D = 0$.

$\langle q_{O_2} \rangle$ (mL/min)	$\langle q_{CO_2} \rangle$ (mL/min)	RQ –	$\langle P^a_{O_2} \rangle$ (mmHg)	$\langle P^a_{CO_2} \rangle$ (mmHg)	$\langle \chi_{O_2} \rangle$ –	$\langle \chi_{CO_2} \rangle$ –	V_D (L)	$V_{\min}$ (L)	$V_{\max}$ (L)
273	−326	1.19	116	36.7	16.3%	5.15%	0	2.50	3.05

TABLE 3. Averaged quantities for a healthy hyperventilating patient.

$\langle q_{O_2} \rangle$ (mL/min)	$\langle q_{CO_2} \rangle$ (mL/min)	RQ –	$\langle P^a_{O_2} \rangle$ (mmHg)	$\langle P^a_{CO_2} \rangle$ (mmHg)	$\langle \chi_{O_2} \rangle$ –	$\langle \chi_{CO_2} \rangle$ –	V_D (L)	$V_{\min}$ (L)	$V_{\max}$ (L)
267	−268	1	108	38.6	15.2%	5.42%	0.233	2.58	2.99

quite similar, and $\langle P^a_{CO_2} \rangle$ and $\langle \chi_{CO_2} \rangle$ are not significantly impacted. We also note that V_D in that situation is higher than in the normal breathing. The evolution of the lung volume with respect to time is given in Figure 8.

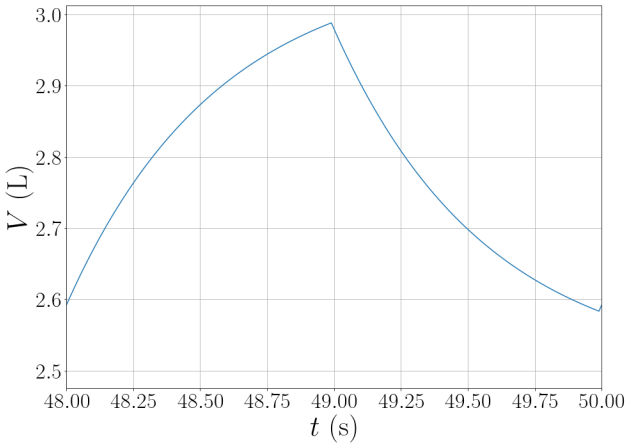

FIGURE 8. Plot w.r.t. time of the total volume V for a healthy hyperventilating patient.

Remark 7. *Compared to the static regime (see Remark 4), in the dynamic one, neglecting the Haldane effect implies a carbon dioxide flux reduction of approximately* 6% *with our model. Note that it may lead to the observation of two adjunct phenomena: a decrease of the carbon dioxide flux which is exhaled, and a decrease of the arterial carbon dioxide pressure (hence an increase between the arterial and venous carbon dioxide pressures). It is related to the fact that the Haldane effect indeed allows greater carbon dioxide exchanges for a given difference between arterial/venous pressures. Even when decreasing this pressure drop, we observe the persistance of the carbon dioxide exchanges, thanks to the influence of oxygen (which binds with hemoglobin, leading to carbon dioxide release).*

5. PARAMETER SENSITIVITY

In order to investigate the behaviour of the model in different cases, we lead a sensitivity analysis with respect to the parameters R, E and D_m. Those parameters can take the following values:

$$R = 2^i R^{\mathrm{h}}, \quad -1 \leq i \leq 4, \qquad E = 2^j E^{\mathrm{h}}, \quad -4 \leq j \leq 4, \qquad D_m = 2^{-k} D_m^{\mathrm{h}}, \quad 0 \leq k \leq 6,$$

remembering that, in any case, we have $D_{m,\mathrm{CO}_2} = 20 D_{m,\mathrm{O}_2}$. We choose to focus only on these parameters since they respectively drive the ventilation and diffusion processes.

5.1. **Global structuration.** To perform this study, 378 numerical simulations of our model were run. For each set of parameters, we plotted colored dots whose coordinates are either $(\langle q_{\mathrm{O}_2}\rangle, \langle q_{\mathrm{CO}_2}\rangle)$ on Figures 9–11a or $(\langle P^a_{\mathrm{O}_2}\rangle, \langle P^a_{\mathrm{CO}_2}\rangle)$ on Figures 9–11b. The red color is associated to R, the green one to E and the blue one to D_m.

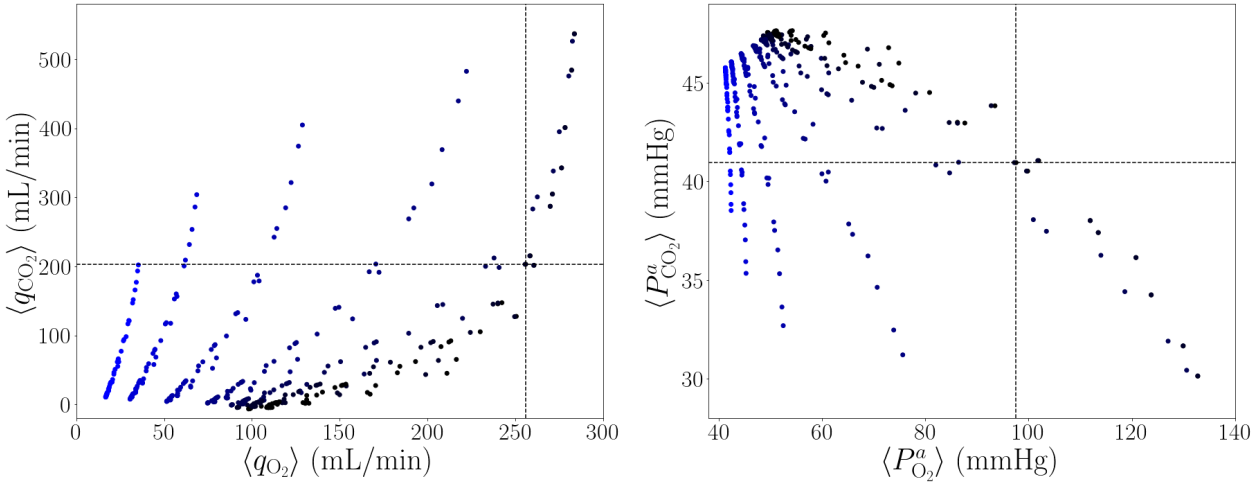

FIGURE 9. Plots with averaged (a) fluxes of O_2 and CO_2, (b) arterial pressures of O_2 and CO_2, with blue-scaled values of the diffusion coefficients D_m.

In Figure 9, light (respectively dark) blue corresponds to the smaller (respectively higher) values of D_m. On the contrary, in Figure 10, light (respectively dark) green corresponds to the higher (respectively smaller) values of E, and the same goes for Figure 11 with the red color.

In each figure, the intersection of the two vertical and horizontal lines provides the healthy reference situation defined in Section 4.

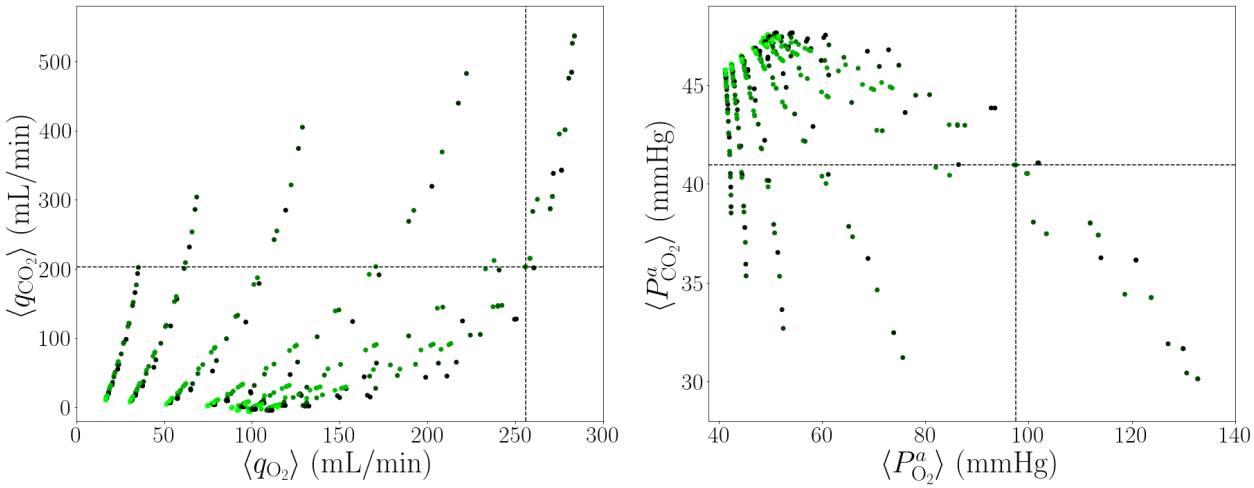

FIGURE 10. Plots with averaged (a) fluxes of O_2 and CO_2, (b) arterial pressures of O_2 and CO_2, with green-scaled values of E.

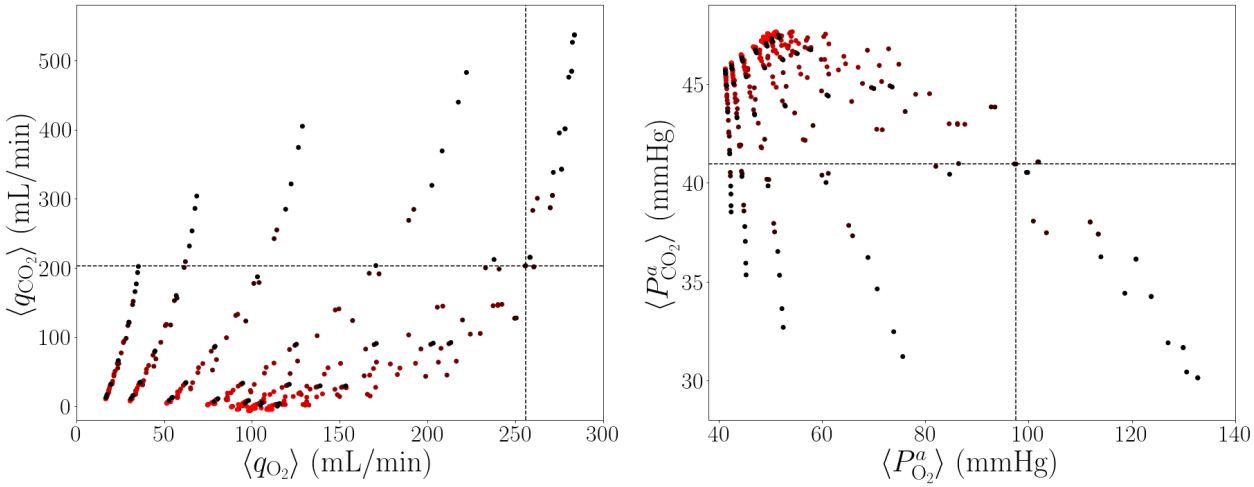

FIGURE 11. Plots with averaged (a) fluxes of O_2 and CO_2, (b) arterial pressures of O_2 and CO_2, with red-scaled values of R.

In all Figures 9–11, with respect to the healthy reference values, there is a quadrant where there is no plotted dot. It seems hypercapnea and hyperoxia cannot simultaneously happen in our model with the chosen range of parameters. We can observe branched patterns with respect to D_m, see Figure 9, whereas there is no clear structure appearing in Figures 10–11 with respect to E or R. In Figure 9, the coefficients D_m seem to drive the behaviour of $\langle P^a_{O_2} \rangle$: $\langle P^a_{O_2} \rangle$ decreases when D_m decrease too.

Moreover, the upper left quadrant of Figures 9–11b corresponds to high values of $\langle P^a_{CO_2} \rangle$ and low values of $\langle P^a_{O_2} \rangle$. They can be obtained in several pathological cases: for large E (fibrosis), or normal E and large R (asthma). For small values of E, which can model emphysema, $\langle P^a_{O_2} \rangle$ is larger than in the normal case and $\langle P^a_{CO_2} \rangle$ is lower: dots are in the lower right quadrant. In this situation, when increasing R, the dots are shifted towards the upper left quadrant. Moreover, decreasing D_m first impacts the oxygen transfer, so that dots are shifted to the left (lower left quadrant) before impacting the carbon dioxide transfer. We also checked that there is no particular structure rising with respect to $\tau = R/E$. To further investigate possible patterns, we separate in Figure 12 the cases when $E \leq E^{\mathrm{h}}$ and $E \geq E^{\mathrm{h}}$ for the dots plotted in Figure 11b. More structures with respect to the resistance value R are observed in particular in the emphysema case: $\langle P^a_{CO_2} \rangle$ increases when R increases too, see Figure 12b.

5.2. **Crossed sensitivity structuring.** In this subsection, we investigate the crossed sensitivity with respect to the parameters (R, E, D_m), by setting one of them at its healthy value and letting the two other vary. We choose the oxygen and carbon dioxide arterial pressures as outputs. Again, remember that D_{m,CO_2} and D_{m,O_2} are always related by $D_{m,CO_2} = 20 D_{m,O_2}$.

Healthy resistance. We first plot $\langle P^a_{O_2} \rangle$ and $\langle P^a_{CO_2} \rangle$ with respect to E, for the considered values of D_m and $R = R^{\mathrm{h}}$ in Figure 13.

When E is close to E^{h}, there is no variation of $\langle P^a_{CO_2} \rangle$ with respect to D_m, which is not the case for $\langle P^a_{O_2} \rangle$. Note moreover that the variations of $\langle P^a_{CO_2} \rangle$ with respect to D_m for each value

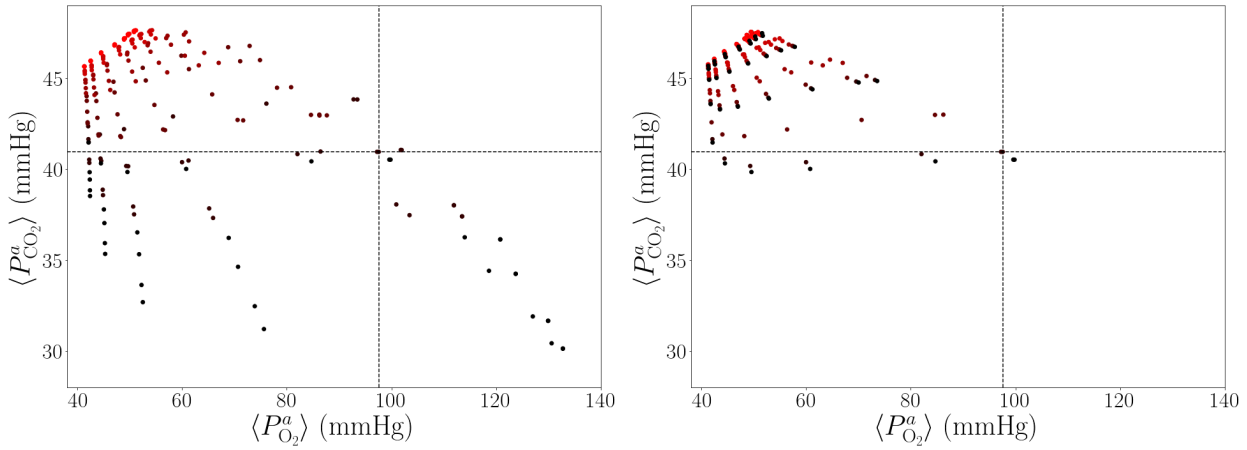

FIGURE 12. Plots with averaged arterial pressures of O_2 and CO_2 for (a) $E \leq E^{\mathrm{h}}$ and (b) $E \geq E^{\mathrm{h}}$, with red-scaled values of R.

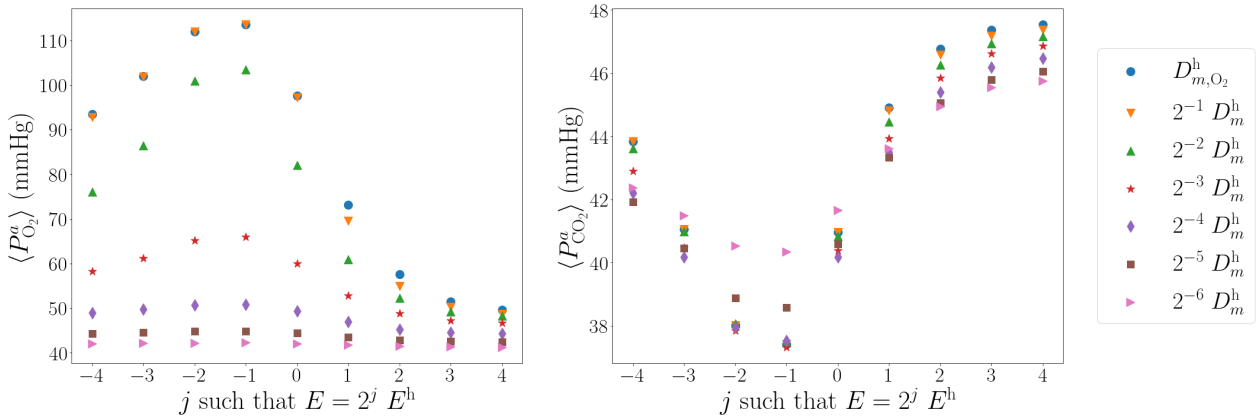

FIGURE 13. Plots of (a) $\langle P^a_{O_2} \rangle$ and (b) $\langle P^a_{CO_2} \rangle$ w.r.t. E, for various diffusion coefficients (with $D_{m,CO_2} = 20 D_{m,O_2}$).

of E are small. This is not the case for $\langle P^a_{O_2} \rangle$, which is sensitive to D_m, in particular when E is smaller than E^{h}. For small degradations of D_m and $E \leq E^{\mathrm{h}}$, we observe moreover a non-monotonic behaviour of $\langle P^a_{O_2} \rangle$ with respect to E: when E decreases, $\langle P^a_{O_2} \rangle$ first increases before decreasing. This phenomenon is due to the fact that the model takes into account the increase of the dead space in pathological situations. Indeed, by considering $V^P_D = 0$, we obtain Figure 14.

Not taking into account the dead space volume increase in emphysema situations implies that the values of arterial pressures for low E are mostly determined by the values of the diffusivities. In particular, a seemingly non-physiological phenomenon rises: $\langle P^a_{O_2} \rangle$ stays at a really high level, when D_m equals $D^{\mathrm{h}}_m/2$ and $D^{\mathrm{h}}_m/4$, even for degraded elastance.

In Figure 15, $\langle P^a_{O_2} \rangle$ and $\langle P^a_{CO_2} \rangle$ are plotted with respect to the D_m parameters, for the various considered values of E. We emphasize again on the fact that we have $D_{m,CO_2} = 20 D_{m,O_2}$ in any situation. We can observe that there is no significant effect of D_m on the variation of $\langle P^a_{CO_2} \rangle$, whereas the jump on $\langle P^a_{O_2} \rangle$ is significant between $D^{\mathrm{h}}_m/4$ and $D^{\mathrm{h}}_m/8$, except for higher values of E, for which $\langle P^a_{O_2} \rangle$ is already very low. More precisely, $\langle P^a_{CO_2} \rangle$ remains close to a constant value for

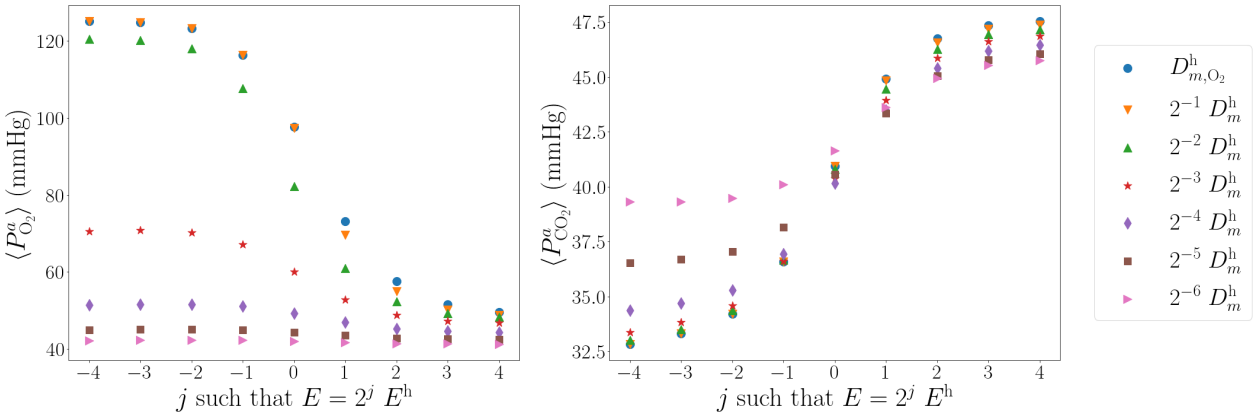

FIGURE 14. Plots of (a) $\langle P^a_{O_2} \rangle$ and (b) $\langle P^a_{CO_2} \rangle$ w.r.t. E, for various diffusion coefficients (with $D_{m,CO_2} = 20 D_{m,O_2}$), when choosing $V^P_D = 0$.

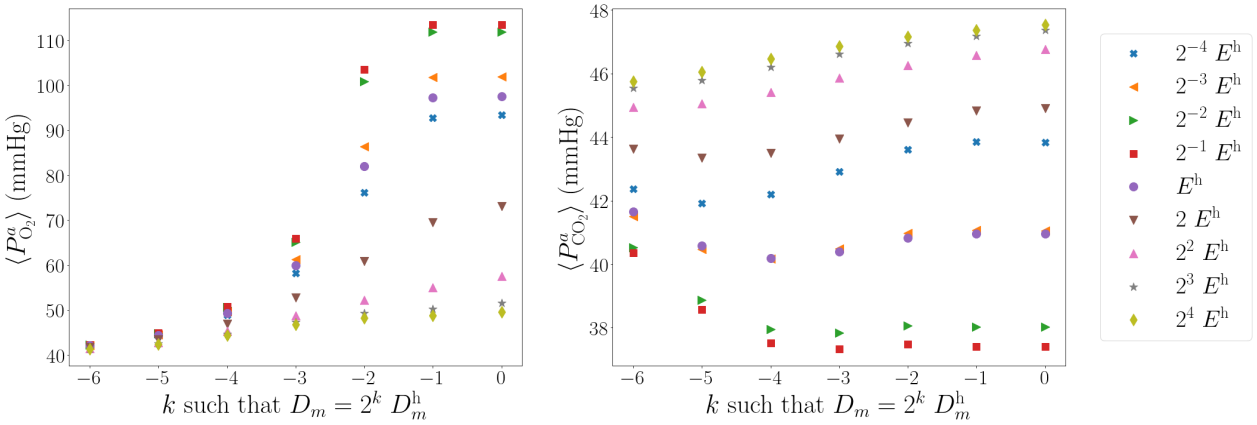

FIGURE 15. Plots of (a) $\langle P^a_{O_2} \rangle$ and (b) $\langle P^a_{CO_2} \rangle$ w.r.t. the D_m parameters, for various E.

each E (excepting larger values of E and degraded values of D_m), so that $\langle P^a_{CO_2} \rangle$ can be seen as a good indicator of lung stiffness. Yet, due to the non-monotonic behaviour with respect to E, the values of $\langle P^a_{CO_2} \rangle$ are nearly the same for $E = E^h$ and $E = E^h/8$.

Healthy diffusion parameters. We now set the D_m coefficients at their healthy values D^h_m. In Figure 16, we consider the variations of $\langle P^a_{O_2} \rangle$ and $\langle P^a_{CO_2} \rangle$ with respect to E, for various R. We observe that, for each value of E, the arterial pressures are monotonic with respect to R: $\langle P^a_{O_2} \rangle$ decreases as R increases, whereas $\langle P^a_{CO_2} \rangle$ increases. When E is large there is almost no variation in the partial pressures with respect to R. When E is lower than E^h, the same nonlinear behaviour as before appears, once again due to the increase of the dead space volume.

In Figure 17, we plot the arterial partial pressures with respect to R. We observe that, for each value of E, they are monotonic in R and they fastly reach a limit value when R increases. There is no monotonicity for a given value of R with respect to E.

Healthy elastance. Finally, we set E at its healthy value E^h, and consider the variations with respect to R and D_m. Figure 18 shows that $\langle P^a_{O_2} \rangle$ and $\langle P^a_{CO_2} \rangle$ are monotonic in R, but not in D_m. Moreover,

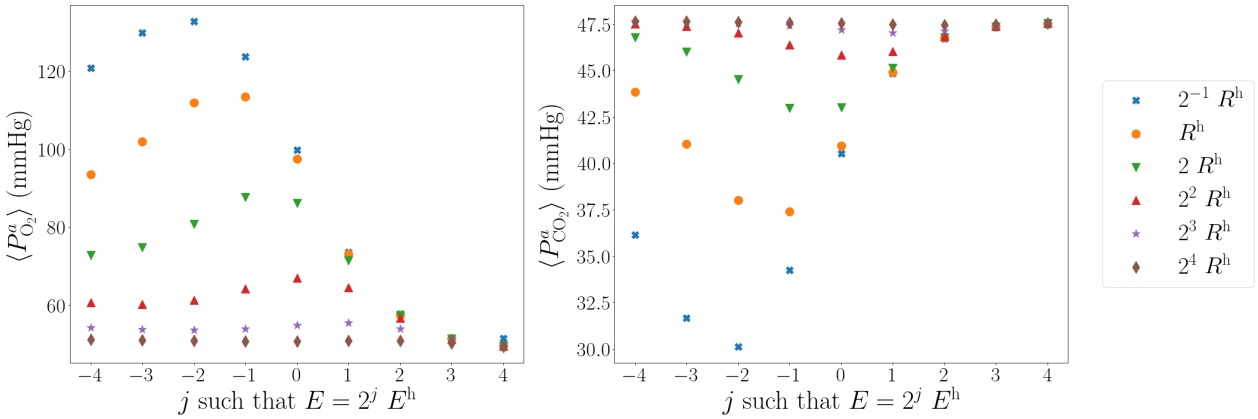

FIGURE 16. Plots of (a) $\langle P^a_{O_2} \rangle$ and (b) $\langle P^a_{CO_2} \rangle$ w.r.t. E, for various R.

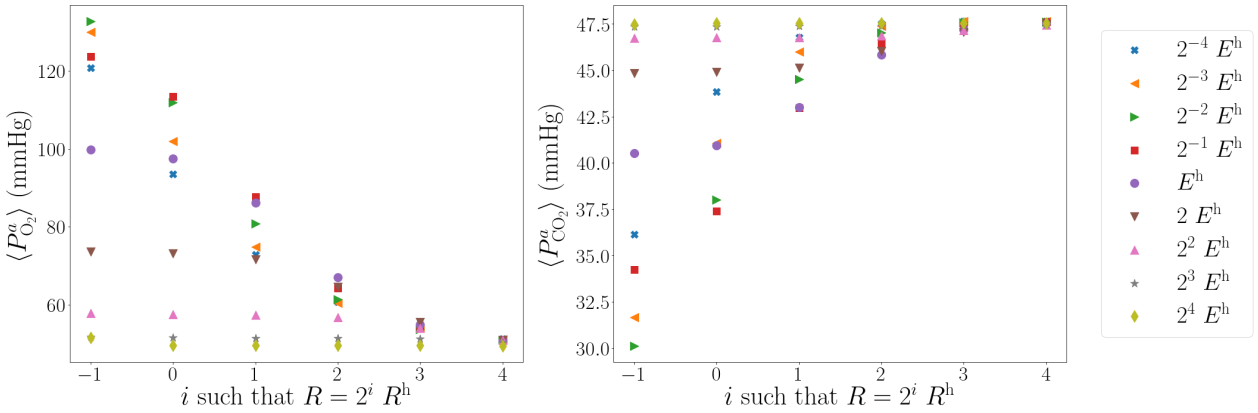

FIGURE 17. Plots of (a) $\langle P^a_{O_2} \rangle$ and (b) $\langle P^a_{CO_2} \rangle$ w.r.t. R, for various E.

$\langle P^a_{O_2} \rangle$ is really sensitive to D_m for values of R close the healthy reference value, and $\langle P^a_{CO_2} \rangle$ has almost a constant value for each R.

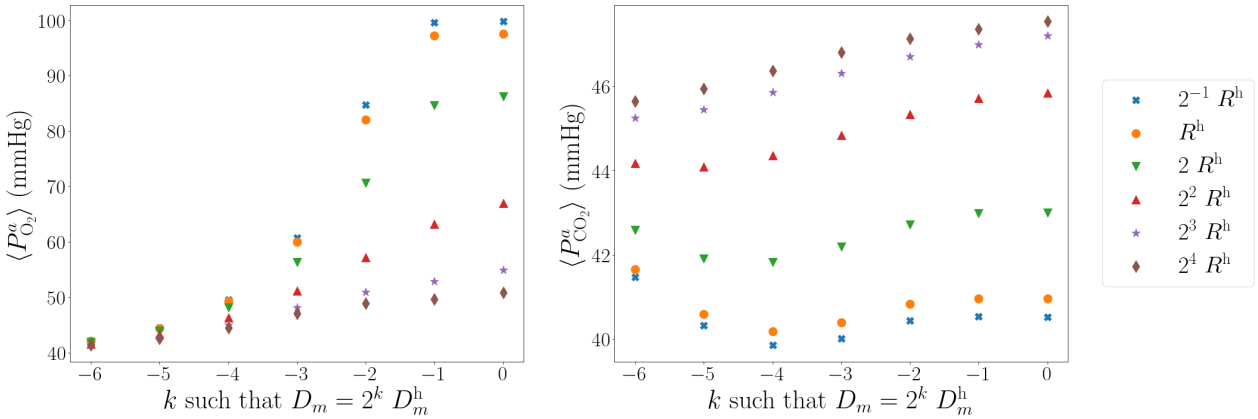

FIGURE 18. Plots of (a) $\langle P^a_{O_2} \rangle$ and (b) $\langle P^a_{CO_2} \rangle$ w.r.t. the D_m parameters, for various R.

To conclude, as expected, the oxygen arterial pressure is more sensitive to the variations of D_m than the carbon dioxide one. Furthermore, taking into account the dead space volume induces some nonlinear effects and non-monotonic behaviour of the arterial pressures. We also observe that highly pathological situations can lead to similar output values, yet the path to those critical values in the parameter space seems to depend on the considered pathologies. Note, however, that, so far, we have used only one breathing scenario. In the next section, we thus further investigate different pathological situations and the effects of different breathing scenarios.

6. Characteristic cases, tendencies

In this section, we exhibit several pathological situations, by varying one or several parameters, illustrating the model ability to recover known qualitative behaviours.

6.1. **Happy hypoxia.** Degrading the D_m parameters, while always keeping $D_{m,\mathrm{CO_2}} = 20\, D_{m,\mathrm{O_2}}$, translates damaging of the membrane where the gaseous exchanges happen. This deterioration numerically induces, in our model, a so-called happy hypoxia effect. Indeed, as we can see in Tables 4–5, compared to Table 1, the oxygen flux drastically drops, and more oxygen is stored in the lung, since the membrane is damaged. The effect on carbon dioxide exchanges is not as significant.

Table 4. Averaged quantities with $D_m = D_m^{\mathrm{h}}/4$.

$\langle q_{\mathrm{O_2}} \rangle$ (mL/min)	$\langle q_{\mathrm{CO_2}} \rangle$ (mL/min)	RQ –	$\langle P^a_{\mathrm{O_2}} \rangle$ (mmHg)	$\langle P^a_{\mathrm{CO_2}} \rangle$ (mmHg)	$\langle \chi_{\mathrm{O_2}} \rangle$ –	$\langle \chi_{\mathrm{CO_2}} \rangle$ –	V_D (L)	$V_{\min}$ (L)	$V_{\max}$ (L)
233	−200	0.858	82	40.8	14.2%	5.65%	0.152	2.50	3.05

Table 5. Averaged quantities with $D_m = D_m^{\mathrm{h}}/8$.

$\langle q_{\mathrm{O_2}} \rangle$ (mL/min)	$\langle q_{\mathrm{CO_2}} \rangle$ (mL/min)	RQ –	$\langle P^a_{\mathrm{O_2}} \rangle$ (mmHg)	$\langle P^a_{\mathrm{CO_2}} \rangle$ (mmHg)	$\langle \chi_{\mathrm{O_2}} \rangle$ –	$\langle \chi_{\mathrm{CO_2}} \rangle$ –	V_D (L)	$V_{\min}$ (L)	$V_{\max}$ (L)
167	−192	1.15	60	40.4	15.5%	5.43%	0.152	2.50	3.05

6.2. **Asthma.** Asthma can be roughly modelled by increasing the resistance of the bronchial tree, since, in particular, it is characterized by some bronchi constriction. In Tables 6–7, we observe that the carbon dioxide flux drastically goes down, whereas the effect on the oxygen flux appears as less significant. Besides, the carbon dioxide exchanges are lowered, leading to rising $\mathrm{CO_2}$ concentrations in both the lung and the blood, and consequently to acidosis ($P^a_{\mathrm{CO_2}} \geq 45$ mmHg). Moreover, we clearly see the decreasing of the total volume amplitude over a breathing period with respect to a healthy patient and thus the increase of the dead space volume.

TABLE 6. Averaged quantities with $R = 2R^{\mathrm{h}}$.

$\langle q_{O_2} \rangle$ (mL/min)	$\langle q_{CO_2} \rangle$ (mL/min)	RQ –	$\langle P^a_{O_2} \rangle$ (mmHg)	$\langle P^a_{CO_2} \rangle$ (mmHg)	$\langle \chi_{O_2} \rangle$ –	$\langle \chi_{CO_2} \rangle$ –	V_D (L)	$V_{\min}$ (L)	$V_{\max}$ (L)
240	−146.	0.607	86.2	43	12.1%	6.03%	0.176	2.53	2.96

TABLE 7. Averaged quantities with $R = 4R^{\mathrm{h}}$.

$\langle q_{O_2} \rangle$ (mL/min)	$\langle q_{CO_2} \rangle$ (mL/min)	RQ –	$\langle P^a_{O_2} \rangle$ (mmHg)	$\langle P^a_{CO_2} \rangle$ (mmHg)	$\langle \chi_{O_2} \rangle$ –	$\langle \chi_{CO_2} \rangle$ –	V_D (L)	$V_{\min}$ (L)	$V_{\max}$ (L)
193	−62.1	0.321	67	45.8	9.40%	6.43%	0.234	2.58	2.85

For strong asthma ($R = 4R^{\mathrm{h}}$ in the cases we study below), the patient can try to adapt his respiration to balance the asthma effect. We investigate two different scenarios.
In the first one, the breathing period is reduced at $T = 2$ s, and the inspiration proportion is increased at $i_{\mathrm{frac}} = 0.5$: we consider again a hyperventilating patient as in Table 3. Table 8 confirms that hyperventilation is not at all a proper response to asthma.
In the second one, we trigger an active expiration, *i.e.* we involve a positive pressure at expiration, namely $P_{\mathrm{ext}}(t) = 2.00$ when $i_{\mathrm{frac}}T \leq t < T$, with $i_{\mathrm{frac}} = 0.35$ and $T = 5$ s again. The respiration improvement is then observed in Table 9, where we recover values very close to the healthy ones in Table 1, in particular because the dead space volume becomes again equal to the anatomical one because of the active expiration process.

TABLE 8. Averaged quantities with $R = 4R^{\mathrm{h}}$ and hyperventilation.

$\langle q_{O_2} \rangle$ (mL/min)	$\langle q_{CO_2} \rangle$ (mL/min)	RQ –	$\langle P^a_{O_2} \rangle$ (mmHg)	$\langle P^a_{CO_2} \rangle$ (mmHg)	$\langle \chi_{O_2} \rangle$ –	$\langle \chi_{CO_2} \rangle$ –	V_D (L)	$V_{\min}$ (L)	$V_{\max}$ (L)
152	−27	0.178	57.6	46.8	8.20%	6.60%	0.374	2.72	2.85

TABLE 9. Averaged quantities with $R = 4R^{\mathrm{h}}$ and active expiration.

$\langle q_{O_2} \rangle$ (mL/min)	$\langle q_{CO_2} \rangle$ (mL/min)	RQ –	$\langle P^a_{O_2} \rangle$ (mmHg)	$\langle P^a_{CO_2} \rangle$ (mmHg)	$\langle \chi_{O_2} \rangle$ –	$\langle \chi_{CO_2} \rangle$ –	V_D (L)	$V_{\min}$ (L)	$V_{\max}$ (L)
253	−197	0.778	95.5	41.2	13.4%	5.77%	0.150	2.10	2.62

6.3. **Pathologies affecting tissue elasticity.**

6.3.1. *Fibrosis.* Increasing elastance E is characteristic of lung fibrosis. In both Tables 10–11, E is chosen as $E = 2E^{\mathrm{h}}$, whereas the D_m parameters are set to their healthy values in Table 10, and to $D^{\mathrm{h}}_m/4$ in Table 11. Indeed, the tissue damage can also have an effect on the diffusivities. The lung volume remains the same in both situations.

TABLE 10. Averaged quantities with $E = 2E^{\mathrm{h}}$.

$\langle q_{\mathrm{O}_2}\rangle$ (mL/min)	$\langle q_{\mathrm{CO}_2}\rangle$ (mL/min)	RQ –	$\langle P^a_{\mathrm{O}_2}\rangle$ (mmHg)	$\langle P^a_{\mathrm{CO}_2}\rangle$ (mmHg)	$\langle \chi_{\mathrm{O}_2}\rangle$ –	$\langle \chi_{\mathrm{CO}_2}\rangle$ –	V_D (L)	$V_{\min}$ (L)	$V_{\max}$ (L)
212	−90.3	0.426	73.2	44.9	10.3%	6.30%	0.150	2.50	2.79

TABLE 11. Averaged quantities with $E = 2E^{\mathrm{h}}$ and $D_m = D_m^{\mathrm{h}}/4$.

$\langle q_{\mathrm{O}_2}\rangle$ (mL/min)	$\langle q_{\mathrm{CO}_2}\rangle$ (mL/min)	RQ –	$\langle P^a_{\mathrm{O}_2}\rangle$ (mmHg)	$\langle P^a_{\mathrm{CO}_2}\rangle$ (mmHg)	$\langle \chi_{\mathrm{O}_2}\rangle$ –	$\langle \chi_{\mathrm{CO}_2}\rangle$ –	V_D (L)	$V_{\min}$ (L)	$V_{\max}$ (L)
170	−89.1	0.525	60.9	44.4	11.4%	6.18%	0.150	2.50	2.79

In any case, the elastance increasing leads to drastically low values of carbon dioxide flux, whereas the diffusivity decreasing reduces the oxygen flux. Consequently, in the acini and in the blood, the concentration and partial pressure of carbon dioxide are too high, and the oxygen one is far too low.

6.3.2. *Emphysema.* When we model emphysema and the subsequent tissue deterioration through elastance decreasing only, we obtain the results from Table 12 for $E = E^{\mathrm{h}}/4$. Note that, if the modification of the dead space volume is not taken into account (namely, by setting $V_D^P = 0$), we obtain non-physiological results with a too high carbon dioxide flux.

TABLE 12. Averaged quantities with $E = E^{\mathrm{h}}/4$.

$\langle q_{\mathrm{O}_2}\rangle$ (mL/min)	$\langle q_{\mathrm{CO}_2}\rangle$ (mL/min)	RQ –	$\langle P^a_{\mathrm{O}_2}\rangle$ (mmHg)	$\langle P^a_{\mathrm{CO}_2}\rangle$ (mmHg)	$\langle \chi_{\mathrm{O}_2}\rangle$ –	$\langle \chi_{\mathrm{CO}_2}\rangle$ –	V_D (L)	$V_{\min}$ (L)	$V_{\max}$ (L)
269.	−287.	1.06	112.	38.0	0.157	0.0533	0.484	2.83	3.88

Emphysema destroys the alveolar tissues and leads to air trapping, implying increasing the dead space volume. Adding a degradation of D_m as $D_m = D_m^{\mathrm{h}}/4$, we obtain the results presented in Table 13, where the values are close to normal ones, confirming that emphysema can be really tricky to detect.

TABLE 13. Averaged quantities with $E = E^{\mathrm{h}}/4$, and $D_m = D_m^{\mathrm{h}}/4$.

$\langle q_{\mathrm{O}_2}\rangle$ (mL/min)	$\langle q_{\mathrm{CO}_2}\rangle$ (mL/min)	RQ –	$\langle P^a_{\mathrm{O}_2}\rangle$ (mmHg)	$\langle P^a_{\mathrm{CO}_2}\rangle$ (mmHg)	$\langle \chi_{\mathrm{O}_2}\rangle$ –	$\langle \chi_{\mathrm{CO}_2}\rangle$ –	V_D (L)	$V_{\min}$ (L)	$V_{\max}$ (L)
259	−283	1.08	100	38.1	15.8%	5.25%	0.484	2.83	3.88

Next, further degrading the diffusion coefficients with $D_m = D_m^{\mathrm{h}}/8$ and still considering $E = E^{\mathrm{h}}/4$, we get the results from Table 14. We see there a serious drop of the oxygen pressure whereas the carbon dioxide pressure is still low. To be able to have an impact on the carbon dioxide pressure, one may increase the resistance and consider for instance $R = 4R^{\mathrm{h}}$. In this case, in Table 15, the effects become very clear, in the same way as in the asthma case, leading to respiratory acidosis.

TABLE 14. Averaged quantities with $E = E^{\mathrm{h}}/4$, and $D_m = D_m^{\mathrm{h}}/8$.

$\langle q_{\mathrm{O}_2}\rangle$ (mL/min)	$\langle q_{\mathrm{CO}_2}\rangle$ (mL/min)	RQ –	$\langle P^a_{\mathrm{O}_2}\rangle$ (mmHg)	$\langle P^a_{\mathrm{CO}_2}\rangle$ (mmHg)	$\langle \chi_{\mathrm{O}_2}\rangle$ –	$\langle \chi_{\mathrm{CO}_2}\rangle$ –	V_D (L)	$V_{\min}$ (L)	$V_{\max}$ (L)
189	−269	1.42	65.2	37.8	16.9%	4.99%	0.484	2.83	3.84

TABLE 15. Averaged quantities with $E = E^{\mathrm{h}}/4$, $D_{m,\mathrm{O}_2} = D^{\mathrm{h}}_{m,\mathrm{O}_2}/4$ and $R = 4R^{\mathrm{h}}$.

$\langle q_{\mathrm{O}_2}\rangle$ (mL/min)	$\langle q_{\mathrm{CO}_2}\rangle$ (mL/min)	RQ –	$\langle P^a_{\mathrm{O}_2}\rangle$ (mmHg)	$\langle P^a_{\mathrm{CO}_2}\rangle$ (mmHg)	$\langle \chi_{\mathrm{O}_2}\rangle$ –	$\langle \chi_{\mathrm{CO}_2}\rangle$ –	V_D (L)	$V_{\min}$ (L)	$V_{\max}$ (L)
131	−290	0.221	53.9	46.4	9.98%	6.47%	0.814	3.16	3.45

7. Conclusion

We propose a nonlinear coupled dynamical model of ventilation-perfusion for oxygen and carbon dioxide, taking into account the Bohr and Haldane effects. We quantitatively recover acknowledged observable values for a healthy patient, and exhibit realistic qualitative behaviours in pathological situations. We also point out that similar output values can be reached from very different sets of input parameters. Those outputs may not allow to discriminate straightforwardly between patients or pathologies. However, since the patient final state results from various successive parameter degradations, our model may help to understand the patient history. Alternatively, it can be used to define other relevant biomarkers as well as breathing scenarios to classify pathological states or histories. We emphasize that it is crucial to accurately model the dead space volume, in particular for asthma and emphysema-like situations, to recover the expected qualitative behaviours.

This first gas exchange model, accounting for both Bohr and Haldane effects, may further be used as a part of more complex ODE or PDE systems, for instance by coupling it to cardiovascular models (through the connection to parameters such as the transit time of a red blood cell in the acinar region τ_b and the capillary volume V_c), or by considering it in a one-dimensional transport-diffusion model of air in the airways. In this case, it would generalize previous works, which only considered oxygen in [19] or without coupling between the two species in [22, 23]. In particular, it is crucial to take into account the transport phenomena to accurately describe the delay that occurs in the gas exchanges, allowing for instance optimisation strategies for breathing scenarios.

Appendix A. Parameters

We shall consider the following set of parameters corresponding to the standard situation of a healthy person at rest, see Table 16.

TABLE 16. Standard values of some physiological parameters.

Mechanical parameters				**Ref.**
Elastance	E	3.5 – 5	$\mathrm{cmH_2O \cdot L^{-1}}$	[10, 4, 5]
Resistance	R	2	$\mathrm{cmH_2O \cdot s \cdot L^{-1}}$	[10, 5]
Functional residual capacity	FRC	3	L	[10, 29, 16]
Anatomical dead space	V_D^A	0.15	L	[34]
Gas exchange parameters				**Ref.**
Reduced atmospheric pressure	P_{atm}	713	mmHg	[10, 5]
Membrane diffusing capacity (O_2)	$D_{m,\mathrm{O_2}}$	21	$\mathrm{mL \cdot min^{-1} \cdot mmHg^{-1}}$	[10, 5]
Membrane diffusing capacity (CO_2)	$D_{m,\mathrm{CO_2}}$	420	$\mathrm{mL \cdot min^{-1} \cdot mmHg^{-1}}$	[10]
Capillary volume	V_c	70	mL	[5, 10, 34]
Transient time of the RBC	τ_b	0.75	s	[34, 14, 5]
Pressure of O_2 in venous blood	$P^v_{\mathrm{O_2}}$	40	mmHg	[34, 10]
Pressure of CO_2 in venous blood	$P^v_{\mathrm{CO_2}}$	46	mmHg	[34, 10]
Concentration of hemoglobin	C_{Hb}	$2.2 \cdot 10^{-3}$	$\mathrm{mol \cdot L^{-1}}$	[12, 5]
Solubility of O_2 in plasma	σ	$1.4 \cdot 10^{-6}$	$\mathrm{mol \cdot L^{-1} \cdot mmHg^{-1}}$	[14, 5]
Dissociation const. of carbonic acid	$\mathrm{p}K_A$	6.1	–	[34]
Concentration of bicarbonate	$C_{\mathrm{HCO_3^-}}$	$24 \cdot 10^{-3}$	$\mathrm{mol \cdot L^{-1}}$	[34]
Observable quantities				**Ref.**
Tidal volume	V_{T}	0.50	L	[34, 29]
Air flow	$\dot{V}$	± 0.50	$\mathrm{L \cdot s^{-1}}$	[34]
Mean alveolar pressure of O_2	$\langle P^a_{\mathrm{O_2}} \rangle$	100	mmHg	[34, 10, 5, 16]
Mean alveolar pressure of CO_2	$\langle P^a_{\mathrm{O_2}} \rangle$	40	mmHg	[34, 10]
Mean alveolar mole fraction of O_2	$\langle \chi_{\mathrm{O_2}} \rangle$	15%	–	[34, 10, 5, 16]
Mean alveolar mole fraction of CO_2	$\langle \chi_{\mathrm{CO_2}} \rangle$	4%	–	[34, 10]
Mean O_2 transfer rate	$q_{\mathrm{O_2}}$	0.25	$\mathrm{L \cdot min^{-1}}$	[34, 10, 33]
Mean CO_2 transfer rate	$q_{\mathrm{CO_2}}$	0.20	$\mathrm{L \cdot min^{-1}}$	[34, 10]

REFERENCES

[1] G. S. Adair. The hemoglobin system. VI. The oxygen dissociation curve of hemoglobin, *J. Biol. Chem.*, 63:529–545 (1925).

[2] L. Baffico, C. Grandmont and B. Maury. Multiscale modeling of the respiratory tract, *Math. Models Methods Appl. Sci.* 20(1): 59–93 (2010).

[3] J. H. T. Bates. *Lung mechanics, an inverse modeling approach*, Cambridge University Press (2009). *The Respiratory System in Equations*, Springer, MS&A (2013).

[4] R. Begin, A. D. Renzetti Jr., A. H. Bigler and S. Watanabe. Flow and age dependence of airway closure and dynamic compliance, *J. Appl. Physiol.*, 38(2):199–207 (1975).

[5] A. Ben-Tal. Simplified models for gas exchange in the human lungs, *J. Theor. Biol.*, 238:474–495 (2006).

[6] L. Berger, R. Bordas, K. Burrowes, V. Grau, S. Tavener and D. Kay. A poroelastic model coupled to a fluid network with applications in lung modelling, *Int. J. Numer. Meth. Biomed. Engng.* 32(1):e02731 (2015).

[7] C. Brighenti, G. Gnudi and G. Avanzolini. A simulation model of the oxygen alveolo-capillary exchange in normal and pathological conditions, *Physiol. Meas.*, 24:261–275 (2003).

[8] L. Cheng, O. Ivanova, H. H. Fan and M. C. K. Khoo. An integrative model of respiratory and cardiovascular control in sleep-disordered breathing. *Respir. Physiol. Neurobiol.* 174:4–28 (2010).

[9] B. J. B. Grant. Influence of Bohr-Haldane effect on steady-state gas exchange, *J. Appl. Physiol. Respir. Environ. Exerc. Physiol.*, 52:1330–1337 (1982).

[10] A. C. Guyton and J. E. Hall. *Textbook of Medical Physiology*, 9th ed., W.B. Saunders Co, Philadelphia (1996).

[11] E. P. Hill, G. G. Power and L. D. Longo. Kinetics of O_2 and CO_2 exchange. In: *Bioengineering aspects of the lung*, 459–514, Dekker, New York, USA (1977).
[12] M. P. Hlastala and A. J. Berger. *Physiology of Respiration*, 2nd ed. Oxford University Press (2001).
[13] M. Ismail, A. Comerford and W. A. Wall. Coupled and reduced dimensional modeling of respiratoy mechanics during spontaneous breathing, *Int. J. Numer. Meth. Biomed. Engng.* 29:1285–1305 (2013).
[14] J. Keener and J. Sneyd. *Mathematical Physiology*, Interdisciplinary Applied Mathematics, Springer (1998).
[15] G. R. Kelman. Digital computer subroutine for the conversion of oxygen tension into saturation, *J. Appl. Physiol.*, 21(4):1375–1376 (1966).
[16] J. D. Kibble and C. Halsey. *Medical Physiology, The Big Picture*, McGraw Hill (2009).
[17] J. A. Loeppky, U. C. Luft and E. R. Fletcher. Quantitative description of whole blood CO_2 dissociation curve and Haldane effect, *Respir. Physiol.*, 51:167–181 (1983).
[18] H. Malte and G. Lykkeboe. The Bohr/Haldane effect: a model-based uncovering of the full extent of its impact on O_2 delivery to and CO_2 removal from tissues, *J. Appl. Physiol.*, 125:916–922 (2018).
[19] S. Martin and B. Maury. Modeling of the oxygen transfer in the respiratory process, *ESAIM Math. Model. Numer. Anal.*, 47(4):935–960 (2013).
[20] B. Maury. *The Respiratory System in Equations*, Springer, MS&A (2013).
[21] F. Meade. A formula for the carbon dioxide dissociation curve, *Br. J. Anaesth.*, 44(6):630 (1972).
[22] F. Noël and B. Mauroy. Interplay between optimal ventilation and gas transport in a model of the human lung, *Front. Physiol.*, 10:488 (2019).
[23] F. Noël, C. Karamaoun, J. Dempsey and B. Mauroy. The origin of the allometric scaling of lung ventilation in mammals, *arXiv, 2005.12362, ver. 6, peer-reviewed and recommended by Peer community in Mathematical and Computational Biology* (2021).
[24] J. M. Oakes, A. L. Marsden, C. Grandmont, S. C. Shadden, C. Darquenne and I. Vignon-Clémentel. Airflow and particle deposition simulations in health and emphysema: from in vivo to in silico animal experiments, *Ann. Biomed. Engng.*, 42(4):899–914, 2014.
[25] N. Pozin, S. Montesantos, I. Katz, M. Pichelin, I. Vignon-Clémentel and C. Grandmont. A tree-parenchyma coupled model for lung ventilation simulation. *Int. J. Numer. Meth. Biomed. Engng.* 33:e2873 (2017).
[26] C. J. Roth, M. Ismail, L. Yoshihara and W. A. Wall. A comprehensive computational human lung model incorporating inter-acinar dependencies: application to spontaneous breathing and mechanical ventilation, *Int. J. Numer. Meth. Biomed. Engng.* 33(1):e02787 (2015).
[27] T. Similowski and J. H. T. Bates. Two-compartment modelling of respiratory system mechanics at low frequencies: gas redistribution or tissue rheology?, *Eur. Respir. J.*, 4:353–358 (1991).
[28] J. L. Spencer, E. Firouztale, and R. B. Mellins. Computational expressions for blood oxygen and carbon dioxide concentrations, *Ann. Biomed. Engng.*, 7:59–66 (1979).
[29] J. Sznitman. Convective gas transport in the pulmonary acinus: comparing roles of convective and diffusive lengths, *J. Biomech.*, 42:789–792 (2009).
[30] A. J. Swan, A. R. Clark and M. H. Tawhai. A computational model of the topographic distribution of ventilation in healthy human lungs, *J. Theor. Biol.* 300:222–231 (2012).
[31] A. J. Swan and M. H. Tawhai. Evidence for minimal oxygen heterogeneity in the healthy human pulmonary acinus, *J. Appl. Physiol.*, 110(2):528–537 (2011).
[32] E. R. Weibel, *The pathway for oxygen*, Harvard University Press (1984).
[33] E. R. Weibel, B. Sapoval and M. Filoche. Design of peripheral airways for efficient gas exchange, *Resp. Phys. Neur.*, 148:3–21 (2005).
[34] J. B. West. *Respiratory Physiology: The Essentials*, Williams & Wilkins (1974).

L.B.: Sorbonne Université, CNRS, Université Paris Cité, Laboratoire Jacques-Louis Lions (LJLL), F-75005 Paris, France
Email address: laurent.boudin@sorbonne-universite.fr

C.G.: Inria, Sorbonne Université, Université Paris Cité, CNRS, Laboratoire Jacques-Louis Lions (LJLL), F-75012 Paris, France
Email address: celine.grandmont@inria.fr

B.G., S.M.: MAP5, CNRS UMR 8145, Université Paris Cité, F-75006 Paris, France
Email address: berenice.grec@u-paris.fr, sebastien.martin@u-paris.fr